nature neuroscience

ARTICLES

https://doi.org/10.1038/s41593-019-0462-8

Stress resilience is promoted by a *Zfp189*-driven transcriptional network in prefrontal cortex

Zachary S. Lorsch[1,10], Peter J. Hamilton[1,10], Aarthi Ramakrishnan[1], Eric M. Parise[1], Marine Salery[1], William J. Wright[2], Ashley E. Lepack[1], Philipp Mews[1], Orna Issler[1], Andrew McKenzie[3], Xianxiao Zhou[3], Lyonna F. Parise[1], Stephen T. Pirpinias[1], Idelisse Ortiz Torres[1], Hope G. Kronman[1], Sarah E. Montgomery[1], Yong-Hwee Eddie Loh[1], Benoit Labonté[4], Andrew Conkey[1], Ann E. Symonds[1], Rachael L. Neve[5], Gustavo Turecki[6,7], Ian Maze[1], Yan Dong[2], Bin Zhang[3], Li Shen[1], Rosemary C. Bagot[6,8,9] and Eric J. Nestler[1*]

Understanding the transcriptional changes that are engaged in stress resilience may reveal novel antidepressant targets. Here we use gene co-expression analysis of RNA-sequencing data from brains of resilient mice to identify a gene network that is unique to resilience. *Zfp189*, which encodes a previously unstudied zinc finger protein, is the highest-ranked key driver gene in the network, and overexpression of *Zfp189* in prefrontal cortical neurons preferentially activates this network and promotes behavioral resilience. The transcription factor CREB is a predicted upstream regulator of this network and binds to the *Zfp189* promoter. To probe CREB–*Zfp189* interactions, we employ CRISPR-mediated locus-specific transcriptional reprogramming to direct CREB or G9a (a repressive histone methyltransferase) to the *Zfp189* promoter in prefrontal cortex neurons. Induction of *Zfp189* with site-specific CREB is pro-resilient, whereas suppressing *Zfp189* expression with G9a increases susceptibility. These findings reveal an essential role for *Zfp189* and CREB–*Zfp189* interactions in mediating a central transcriptional network of resilience.

Stressful life events contribute to the risk for developing major depressive disorder (MDD). However, most stress-exposed individuals do not develop MDD. Understanding the biological basis of such stress resilience may illuminate causal mechanisms underlying MDD and reveal novel therapeutic targets for this disorder.

The chronic social defeat stress (CSDS) paradigm in mice is a widely used and reliable model in which to explore the biological basis of stress resilience, wherein a proportion of stressed animals display behavior that mimics characteristics of MDD (termed 'susceptible'), while the remainder do not (termed 'resilient')[1,2]. CSDS therefore recapitulates the divergence in stress responses observed in humans. Importantly, resilience is not simply the absence of susceptibility, but rather an active homeostatic response to stress that involves broad transcriptional changes across brain regions. In fact, far more early transcriptional changes are observed in stress-resilient than in stress-susceptible mice[2,3]. However, the relationship among different genes that have been found to be altered in the resilient brain, as well as their mechanistic regulation, have not been determined.

By clustering genes into units (modules) based on coordinated transcriptional regulation, network-based analytical methods such as weighted gene co-expression network analysis (WGCNA) provide an alternative approach to standard differential expression analysis of large transcriptional datasets. WGCNA has been used to define gene networks from RNA-sequencing (RNA-seq) of human postmortem brain samples in complex disorders such as schizophrenia[4], Parkinson's disease[5], Alzheimer's disease[6], autism[7] and MDD[8,9]. However, because these studies involve in silico analyses of human brain RNA-seq data, the causality of the inferred relationships cannot be determined through in vivo experiments. Recent studies using mice have circumvented this problem by identifying stress-susceptibility networks that are dependent on the expression of key module hub genes, which, when manipulated in vivo, affect both module gene expression and overall stress susceptibility[3,8]. However, the transcriptional organization of the quantitatively larger and translationally relevant resilient response remains entirely unexplored. Moreover, there is currently no understanding of how regulatory factors act on central driver genes to activate key transcriptional networks. This knowledge may yield novel targets for more effective MDD therapeutics.

Here, we reveal that *Zfp189*, a gene that encodes a putative zinc finger transcription factor that has not been previously implicated in stress, controls a transcriptionally active network that is unique to the resilient phenotype. We show that manipulating *Zfp189* in the prefrontal cortex (PFC) preferentially affects expression of this network as well as resilience behavior. We also employ clustered regularly interspaced short palindromic repeats (CRISPR) and Cas9

[1]Nash Family Department of Neuroscience, Friedman Brain Institute, Icahn School of Medicine at Mount Sinai, New York, NY, USA. [2]Department of Neuroscience, University of Pittsburgh, Pittsburgh, PA, USA. [3]Department of Genetics and Genomic Sciences, Icahn School of Medicine at Mount Sinai, New York, NY, USA. [4]Department of Neuroscience and Psychiatry, Laval University, Québec City, Québec, Canada. [5]Gene Delivery Technology Core, Massachusetts General Hospital, Cambridge, MA, USA. [6]Department of Psychiatry, McGill University, Montréal, Québec, Canada. [7]McGill Group for Suicide Studies, Douglas Mental Health University Institute, McGill University, Montréal, Québec, Canada. [8]Department of Psychology, McGill University, Montréal, Québec, Canada. [9]Ludmer Centre for Neuroinformatics and Mental Health, Montréal, Québec, Canada. [10]These authors contributed equally: Zachary S. Lorsch, Peter J. Hamilton. *e-mail: Eric.Nestler@mssm.edu

with no functional moiety (dCas9) to illustrate the regulation of this network. We demonstrate that cyclic AMP (cAMP) response element (CRE) binding protein (CREB), a well-studied transcription factor, binds to the *Zfp189* locus to induce *Zfp189*, which triggers downstream gene network activity and increases resilience. Taken together, these data provide a functional characterization of the transcriptional changes involved in resilience, identify *Zfp189* as an important molecular regulator of resilience and demonstrate the higher-order mechanism by which upstream regulators interact with in-network key driver genes to regulate large transcriptional networks that direct complex behavior.

Results

***Zfp189* regulates a resilient-specific transcriptional network.** To identify transcriptional changes associated with stress resilience, we integrated WGCNA and differential expression data from our recently published[3] RNA-seq dataset of mice following CSDS (Fig. 1a). WGCNA of the resilient phenotype, which had not been previously explored, revealed 30 modules present across the following four brain regions: the PFC, the ventral hippocampus (vHIP), the nucleus accumbens (NAc) and the basolateral amygdala (BLA) (Fig. 1b). To confirm the validity of this approach, we looked for the presence of known biological relationships within the modules via protein–protein interactions (PPIs) and found 12 modules in which known PPIs were greater than expected by chance (Supplementary Fig. 1a). To determine the relevance of these networks to human MDD, we examined whether the CSDS-associated resilience modules are preserved in RNA-seq data from postmortem samples from patients with MDD[8]. A total of 56.6% of our modules were preserved in human brain, but—consistent with a role in resilience—more modules (11 versus 2) showed greater preservation in control conditions than in MDD (Supplementary Fig. 1b–e).

To identify modules that were specific to the resilient phenotype, we used module differential connectivity (MDC) analysis[6] to analyze whether each resilient module was similarly structured when the module genes were analyzed using parallel RNA-seq data from susceptible mice and unstressed controls[3]. We also used enrichment analysis to determine the degree to which each resilient module contains differentially expressed genes (DEGs) in each of the four brain regions studied 48 h after CSDS. To identify networks that were both resilient-specific and transcriptionally active, we combined these approaches (Fig. 1b). Only two modules, pink and brown, were enriched for DEGs across brain regions. While brown module connectivity was distinct from susceptible conditions (MDC = 0.9) but not from control conditions, pink module connectivity was distinct from both susceptible (MDC = 0.89) and control (MDC = 0.91) conditions. Therefore, of the 30 modules generated from the four brain regions of resilient mice, only the pink module is unique to the resilient phenotype and transcriptionally active across brain regions. Importantly, the pink module was both enriched for known molecular interactions and more strongly preserved in human controls ($P = 1.07 \times 10^{-17}$) than in human MDD ($P = 1.14 \times 10^{-15}$) (Supplementary Fig. 1).

To determine the structure of the pink module, we reconstructed the network on the basis of individual gene–gene correlations and predicted gene regulators as previously described[10,11] (Fig. 1c). A total of 40 network genes met the criteria for key drivers (Supplementary Table 1). Of these, the strongest key driver gene was *Zfp189*, which contains 52 defined connections and is tightly integrated in the core network (Supplementary Fig. 2a,b). To determine the relationship between key driver genes and the overall network response, we compared individual differential expression patterns of *Zfp189* and the other top ten key driver genes of the pink module to module DEGs across brain regions (Fig. 1d; Supplementary Fig. 2c). Only *Zfp189* was differentially expressed (upregulated in the PFC of resilient mice) and recapitulated the brain-region-specific DEG enrichment profile of the pink module (also upregulated in the PFC of resilient mice). As the PFC has been implicated in stress resilience[12], *Zfp189* may act in this brain region to drive stress resilience through the resilient-unique pink module. While Zfp189 has not been previously implicated in any neurobiological context, it is a Krüppel-associated box (KRAB) protein[13] and its human ortholog *ZNF189* has been shown to directly bind to DNA[14], which suggests that Zfp189 may function as a transcription factor.

***Zfp189* in the PFC exerts pro-resilient and antidepressant-like actions.** To explore the role of *Zfp189* in human resilience, we performed quantitative PCR (qPCR) to evaluate the expression of its ortholog *ZNF189* in the PFC of human postmortem brains (Supplementary Table 2). We found that *ZNF189* mRNA is

Fig. 1 | Identification of the resilient-specific pink module and its pro-resilient top key driver *Zfp189*. a, Overview of the CSDS protocol, SI test phenotyping, brain dissections and RNA-seq analysis of the four brain regions (PFC, NAc, BLA and vHIP) used to identify resilient-specific transcriptional networks. **b**, Resilient modules (colored bars) identified by WGCNA. Modules, named with an arbitrary color (outer most ring) are ranked clockwise by overall DEG enrichment ($P < 0.05$, fold change (FC) > 1.3). Phenotype specificity as determined by resilient (RES) MDC in susceptible (SUS) and control (CON) networks and DEG enrichment is displayed internally. Presence of MDC color denotes statistical significance (FDR $q < 0.05$). DEG enrichments are scaled by $-\log_{10}(P \text{ value})$ with only significant ($P < 0.05$) enrichments featured in color. The pink module (top) is the only module that shows DEGs across brain regions and MDC when compared with both susceptible and control mice. Modules were generated from $n = 44$ RNA-seq libraries consisting of pooled brain samples with DEG enrichment assessed via a Fisher's exact test with Benjamini–Hochberg FDR correction for multiple comparisons as indicated**. c**, Network structure of the pink module. Key drivers are featured and scaled in size according to the number of connections in the network. *Zfp189* is the top key driver gene. **d**, Correspondence between differential expression for the individual *Zfp189* transcript and DEG enrichment for the pink module as a whole across phenotypes and brain areas. DEG enrichments are scaled by $-\log_{10}(P \text{ value})$ with only significant ($P < 0.05$) enrichments featured in color. In the PFC, both *Zfp189* and the pink module are only affected in animals resilient to CSDS (both upregulated). **e**, mRNA of *ZNF189*, the human ortholog of *Zfp189*, is reduced in postmortem PFC samples from patients with MDD (two-tailed Mann–Whitney, $U = 110.0$, $P = 0.0291$, $n = 17$ (control) and 22 (MDD)). **f**, Experimental timeline to characterize behavioral effects of virally overexpressing *Zfp189* in the PFC before CSDS. **g**, Pro-resilient behavioral effects of *Zfp189* in SI tests. Mice injected intra-PFC with HSV-*Zfp189* and exposed to CSDS spend more time in the interaction zone when a target mouse is present than defeated HSV-GFP mice (mixed model ANOVA, interaction $F_{1,40} = 8.501$, $P = 0.006$, from left to right in the figure panel: $n = 9$, 10, 12 and 13 mice, Bonferroni post-test $P < 0.01$). **h**, Mice overexpressing *Zfp189* in the PFC have an elevated preference for sucrose relative to HSV-GFP mice (two-way ANOVA, $F_{1,41} = 5.102$, $P = 0.029$, from left to right in the figure panel: $n = 9$, 12, 10 and 14 mice). **i**, Experimental timeline to determine behavioral effects of overexpressing *Zfp189* in the PFC in CSDS-susceptible mice. **j**, *Zfp189* reverses depression-like social withdrawal in susceptible mice. Susceptible mice injected intra-PFC with HSV-*Zfp189* spend more time in the interaction zone when the target mouse is present in the post-injection post-test than the pre-injection pre-test, but HSV-GFP injection does not change behavior (mixed model ANOVA, interaction $F_{1,23} = 5.634$, $P = 0.026$, $n = 11$ HSV-GFP and 13 HSV-*Zfp189* mice, Bonferroni post-test $P < 0.001$). **k**, Previously susceptible mice injected with HSV-*Zfp189* have a higher sucrose preference than previously susceptible mice injected with HSV-GFP (two-tailed Mann–Whitney, $U = 29.0$, $P = 0.025$, $n = 11$ (HSV-GFP) and 12 (HSV-*Zfp189*) mice). $^*P < 0.05$, $^{**}P < 0.01$, $^{***}P < 0.001$. Bar graphs show the mean ± s.e.m.

reduced in human MDD samples compared with those from control subjects (Fig. 1e). By examining previous data of RNA expression across mouse cortical cell types[15], we found that *Zfp189* was highly enriched in neurons. We corroborated these data by performing RNAscope on sections from mouse PFC, and observed that a large majority (80.3 ± 5.6%; $n = 3$) of cells expressing *Zfp189*

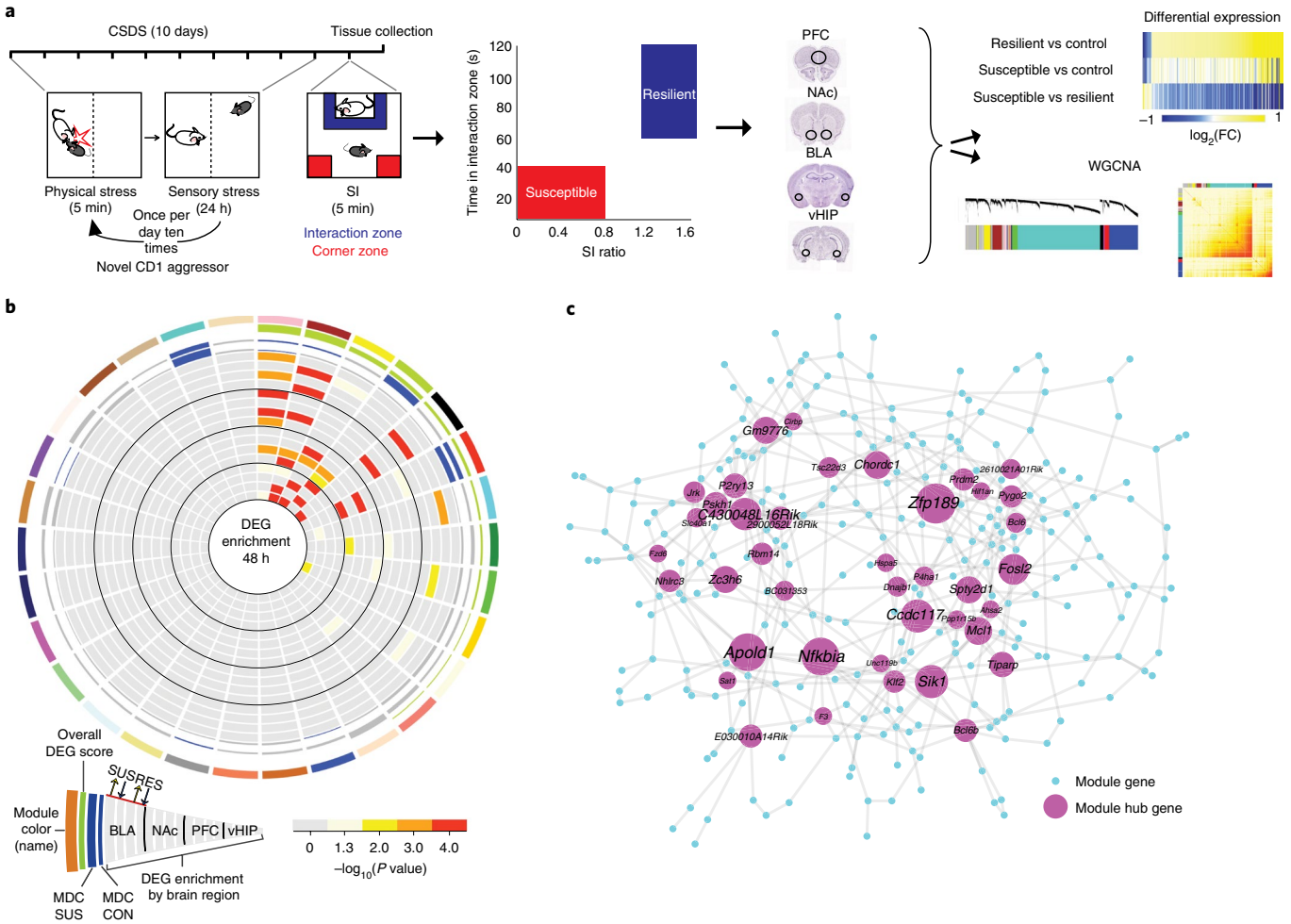

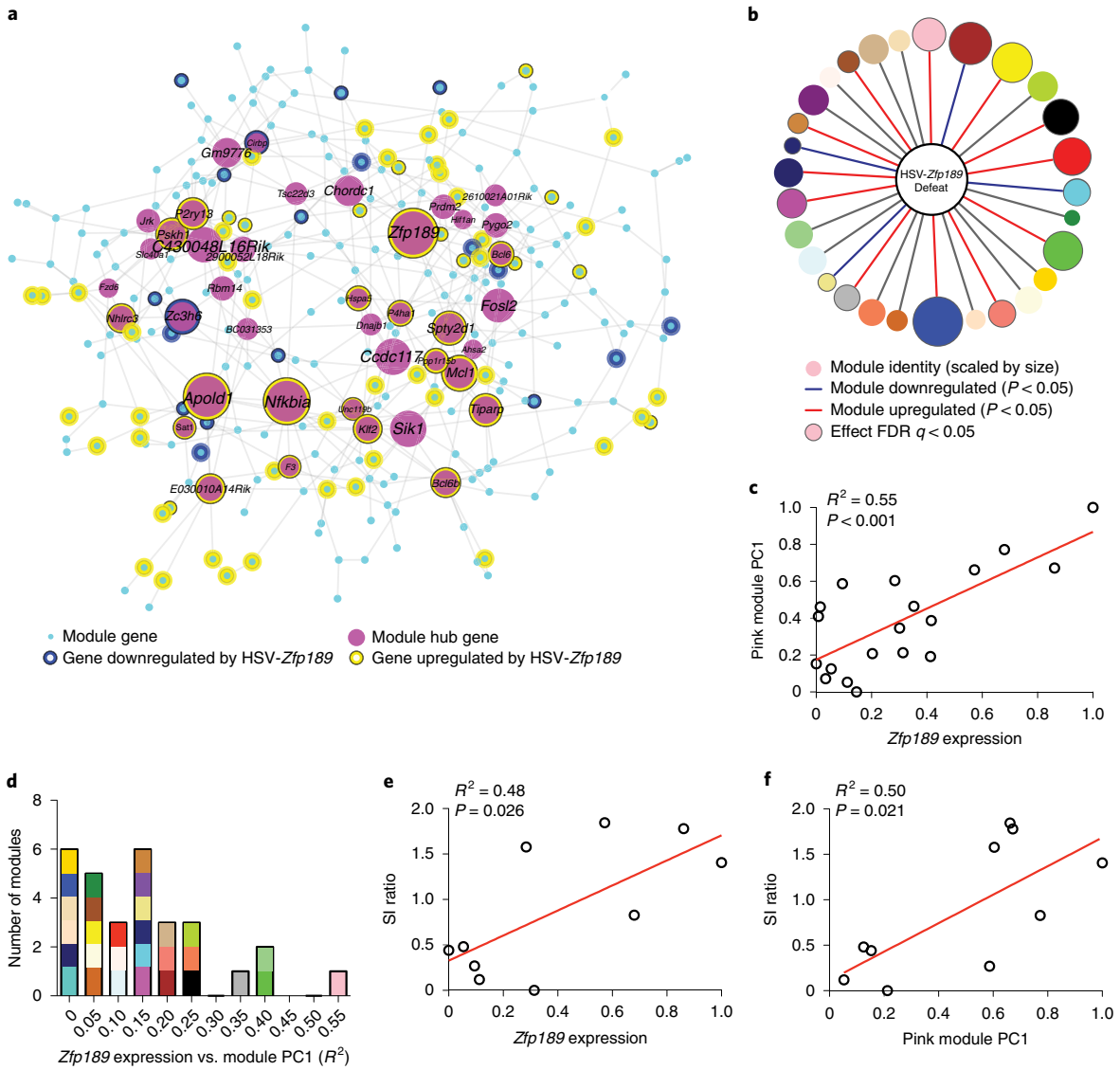

Fig. 2 | Antidepressant-like effects of *Zfp189* associate with pink module expression changes. a, Pink module genes are differentially expressed ($P < 0.05$, $\log_2(FC) > |0.2|$) in the PFC following reversal of susceptibility with HSV-*Zfp189*. $n = 10$ RNA-seq libraries consisting of unpooled PFC from 5 stressed HSV-GFP and 5 stressed susceptible to resilient HSV-*Zfp189* mice. **b**, Module-wide enrichment for HSV-*Zfp189* overexpression in the PFC in previously susceptible mice. Enrichment is determined via multinomial logistic regression with Benjamini–Hochberg FDR correction for multiple comparisons as indicated. **c**, Variations in *Zfp189* predict the PC1 of pink module expression. Linear regression, $n = 19$ RNA-seq libraries consisting of unpooled PFC from 5 stressed HSV-GFP, 4 unstressed HSV-GFP, 5 stressed susceptible to resilient HSV-*Zfp189* and 5 unstressed HSV-*Zfp189* mice. **d**, Histogram of the coefficient of determination (R^2) from linear regression analysis examining the relationship between *Zfp189* expression and the PC1 of each resilient module (modules are plotted accordingly and represented by color). Of all resilient modules, *Zfp189* shows the strongest regulation of the pink module. **e**,**f**, Linear regression showing a positive relationship between resilient behavior and *Zfp189* levels (**e**) in the PFC of each mouse and pink module expression (**f**) ($n = 10$ RNA-seq libraries consisting of 5 stressed HSV-GFP and 5 stressed susceptible to resilient HSV-*Zfp189* mice).

mRNA are neurons (Supplementary Fig. 3a). Therefore, to probe the causal role of *Zfp189* in stress resilience, we used herpes simplex virus (HSV) vectors, which selectively target neurons (Supplementary Fig. 3b), to overexpress *Zfp189* in PFC neurons and then exposed mice to an accelerated social defeat paradigm (Fig. 1f; Supplementary Fig. 4a).

In the social interaction (SI) test, defeated mice overexpressing *Zfp189* in the PFC spent more time interacting with a social target than defeated mice expressing control HSV-green fluorescent protein (GFP) (Fig. 1g). To determine whether this effect extends to other measures of behavior associated with depression- or anxiety-like phenotypes, we analyzed mice in the open-field test (OFT), forced-swim test (FST) and sucrose preference test. In OFTs, unlike controls, HSV-*Zfp189* mice did not show stress-induced anxiety-like effects (Supplementary Fig. 4b,c) and, while there were no differences in the FST results (Supplementary Fig. 4d), HSV-*Zfp189* mice consumed significantly more sucrose than defeated controls (Fig. 1h). Together, these results are consistent with *Zfp189* having a role in the PFC to increase resilience to CSDS.

Since antidepressant treatment is initiated after a diagnosis of MDD, molecular targets that reverse behavioral phenotypes seen in depression have higher therapeutic potential than targets that only prevent susceptibility. We therefore explored the antidepressant potential of *Zfp189* by determining whether CSDS-induced alterations in behavior could be reversed (Fig. 1i). Delivering *Zfp189* to the PFC after CSDS reversed stress-induced social deficits (Fig. 1j).

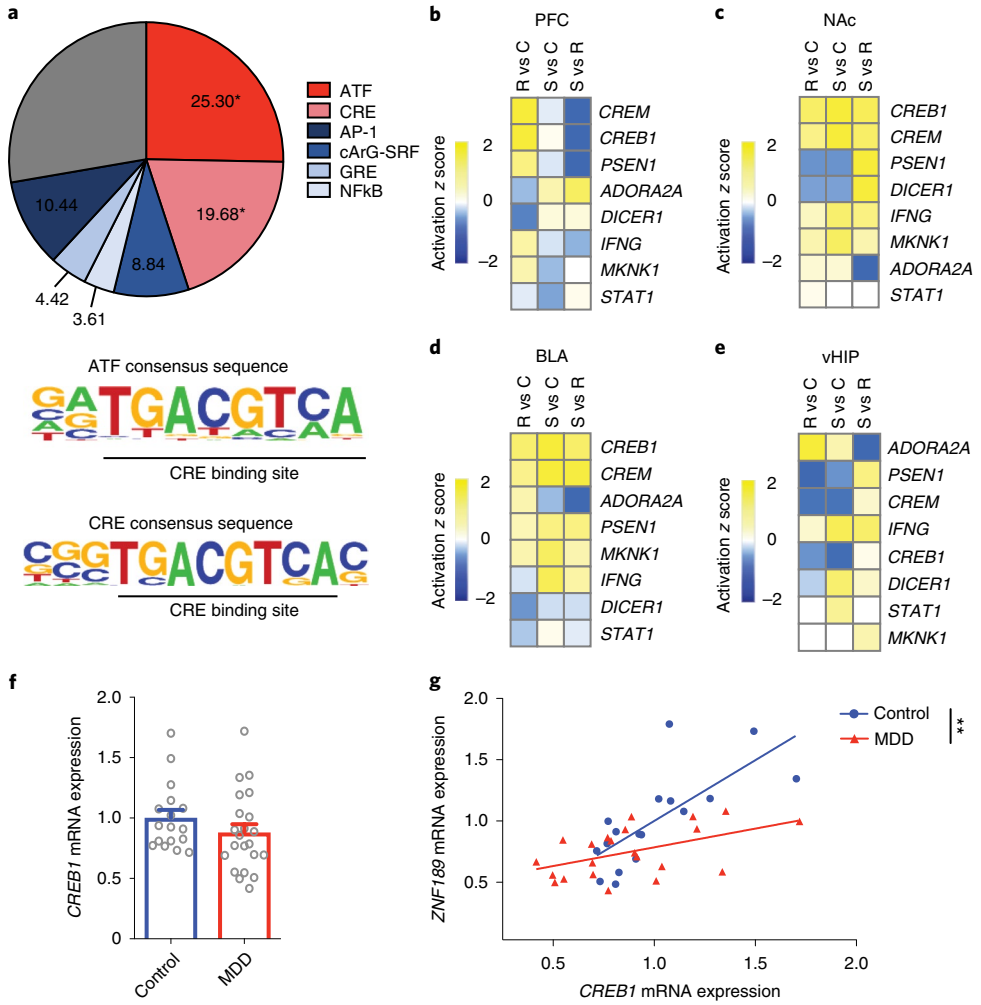

Fig. 3 | CREB is an upstream regulator of the pink module. a, Binding motifs overrepresented (FDR $q < 0.05$) in the pink module with common non-overrepresented motifs (shaded blue) included for comparison (upper). Both significantly overrepresented binding motifs (indicated with asterisks) contain a CRE site (lower). **b**–**e**, Upstream regulator analysis of transcriptional changes in pink module genes in the PFC (**b**), NAc (**c**), BLA (**d**) and vHIP (**e**). CREB is an upstream regulator across brain regions and is predicted to be upregulated in resilience (R) versus control (C) conditions in the PFC. **f**, mRNA levels of *CREB1* in the PFC from patients with MDD and matched controls (two-tailed *t*-test, $t = 1.216$, $P = 0.232$, $n = 17$ (control) and 22 (MDD) samples). **g**, *CREB1* and *ZNF189* are correlated in the PFC of controls to a greater extent than in MDD subjects (ANCOVA, $F_{1,35} = 7.702$, $P = 0.009$, $n = 17$ (control) and 22 (MDD) samples). $^{**}P < 0.01$. Bar graphs show the mean ± s.e.m.

While *Zfp189* overexpression in susceptible mice did not affect OFT, locomotor testing or FST (Supplementary Fig. 4e–g) outcomes, HSV-*Zfp189* mice displayed higher sucrose preference than HSV-GFP mice (Fig. 1k). Thus, *Zfp189* overexpression in the PFC exerts both pro-resilient and antidepressant-like actions.

To test the effects of *Zfp189* on gene expression profiles, we microdissected virally infected tissue and performed RNA-seq. Overexpression of *Zfp189* in PFC neurons upregulated 33.1% (93) of pink module genes, including 47.5% (19) of key driver genes (Fig. 2a). Many of these genes were tightly integrated in the network structure, including *Nfkbia* and *Apold1*, the two top key driver genes after *Zfp189*. Downregulation was less prominent: 7.1% (20) of genes overall and only 5.0% (2) of hub genes. While *Zfp189* overexpression in the PFC of previously susceptible mice significantly downregulated 4 and upregulated 12 resilient modules (Fig. 2b), in support of *Zfp189* inducing behavioral resilience specifically through the pink module, *Zfp189* overexpression in the PFC significantly upregulated the pink module in both previously susceptible (false discovery rate (FDR) $q = 1.67 \times 10^{-12}$) and non-defeated control (FDR $q = 2.63 \times 10^{-4}$; Supplementary Fig. 5) mice.

We next tested whether *Zfp189* overexpression in PFC neurons preferentially affects the pink network. To do this, we performed principal component analysis to determine pink module expression across HSV-*Zfp189* and HSV-GFP samples in both unstressed and defeated groups. Because there is variability in the degree to which *Zfp189* is overexpressed by our HSV method (Supplementary Fig. 4a), we can leverage this variance to determine whether mice in which *Zfp189* was expressed to a higher extent had stronger activation of the pink module and more resilient behavior. Notably, while this relationship between *Zfp189* and the pink module is inherent in the RNA-seq data used to generate the pink module (Fig. 1b,c), there is no a priori relationship between the pink module in our HSV-*Zfp189* sequencing data. As such, our finding that levels of *Zfp189* expression in each PFC sample significantly explained the variation in pink module expression as measured by the first principal component (PC1) ($R^2 = 0.55$, $P < 0.001$; Fig. 2c), independently validates the inherent biological relationship between *Zfp189* and pink module genes that we originally identified in our WGCNA (Fig. 1c). Additionally, while WGCNA is undirected, in the current analysis, overexpression of *Zfp189* is a product of viral transduction, and thus

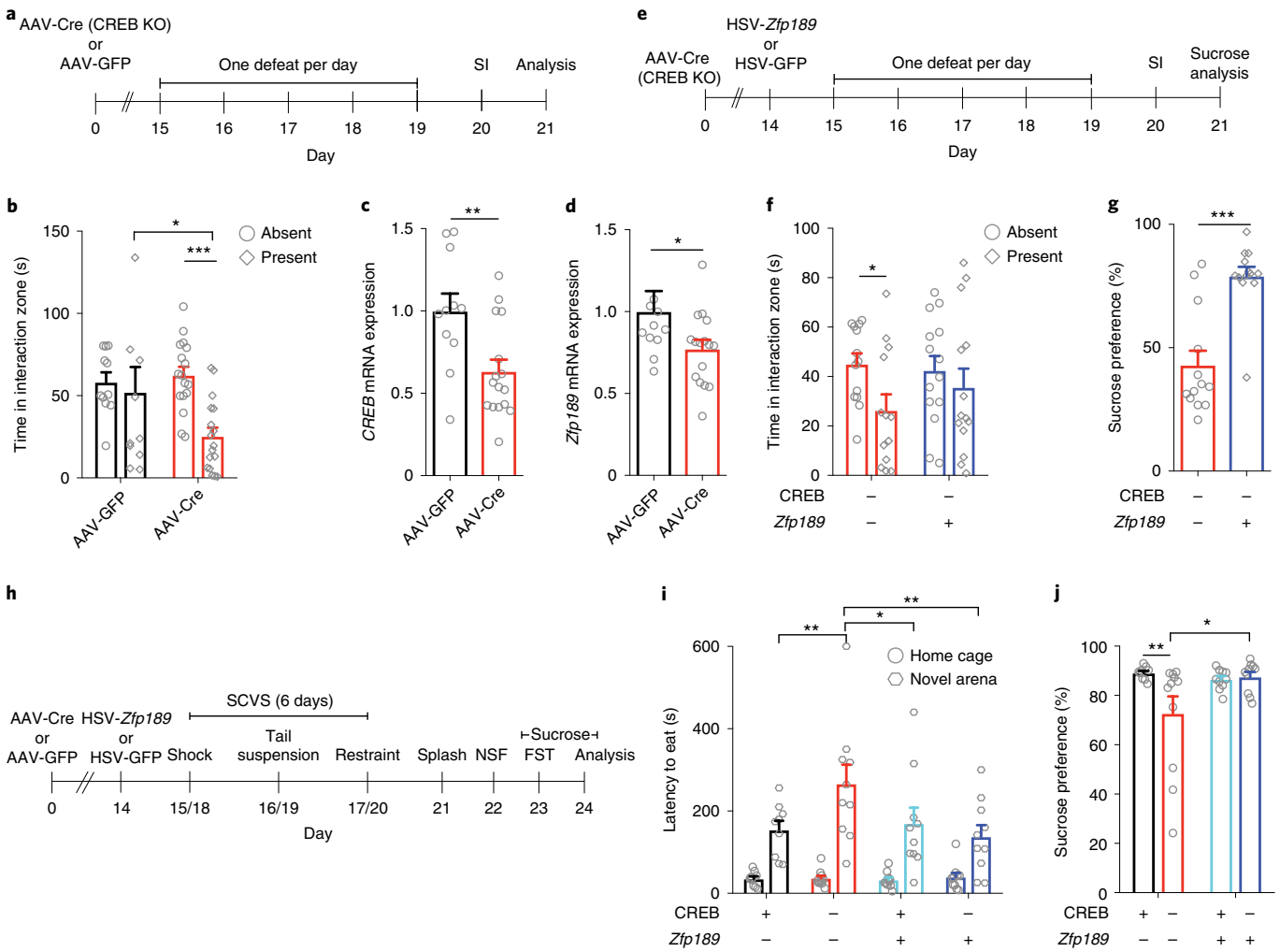

Fig. 4 | CREB KO in the PFC increases susceptibility but is rescued by *Zfp189* overexpression. a, Experimental timeline to evaluate behavioral effects of CREB KO in the PFC. **b**, Local KO of CREB in the PFC produces social avoidance in SI tests in a subthreshold social defeat procedure (mixed model ANOVA, interaction $F_{1,26}=4.656$, $P=0.040$, $n=11$ (AAV-GFP) and 17 (AAV-Cre) mice, Bonferroni post-test $P<0.001$). **c**,**d**, CREB KO reduces mRNA levels of *Creb1* (**c**) (two-tailed *t*-test, $t=2.974$, $P=0.006$) and *Zfp189* (**d**) (two-tailed Mann–Whitney, $U=45.0$, $P=0.036$), $n=11$ (AAV-GFP) and 16 (AAV-Cre) mice. **e**, Experimental timeline to determine whether *Zfp189* overexpression in the PFC reverses the deleterious effects of CREB KO. **f**, CREB KO in the PFC produces social avoidance in the SI test, but concurrent overexpression of *Zfp189* reverses this deficit (mixed model ANOVA, target $F_{1,25}=5.690$, $P=0.025$, from left to right in figure panel: $n=13$ and 14 mice, Bonferroni post-test $P<0.05$). **g**, Overexpression of *Zfp189* in the PFC increases sucrose preference in CREB KO mice (two-tailed *t*-test, $t=5.176$, $P<0.001$, $n=13$ mice). **h**, Experimental schematic for female SCVS to investigate behavioral effects of CREB KO and *Zfp189* overexpression in the PFC. **i**, CREB KO in the PFC increases latency to eat in the novel arena, but not when CREB KO is paired with *Zfp189* overexpression (mixed model ANOVA, interaction $F_{1,35}=5.301$, $P=0.027$, from left to right in figure panel: $n=9$, 11, 10 and 10 mice, Bonferroni post-test compared to CREB$^-$*Zfp189*$^-$ in novel arena, $P<0.01$ for CREB$^+$*Zfp189*$^-$, $P<0.01$ for CREB$^-$*Zfp189*$^+$, and $P<0.05$ for CREB$^+$*Zfp18*$^+$). **j**, Mice with local KO of CREB in PFC have a lower sucrose preference than control mice, an effect blocked by concurrent *Zfp189* overexpression (Kruskall–Wallis test, $\chi^2(3)=8.475$, $P=0.037$, from left to right in figure panel: $n=9$, 11, 10 and 10 mice, two-tailed Mann–Whitney post-test $P=0.009$ for local KO of CREB and $P=0.029$ for overexpression of *Zfp189* with concurrent CREB KO). $^*P<0.05$, $^{**}P<0.01$, $^{***}P<0.001$. Bar graphs show the mean ± s.e.m.

establishes a true causal link between *Zfp189* expression and regulation of the pink module. To determine whether this causal relationship was unique to the pink module, we applied a similar approach to all other modules. Strikingly, *Zfp189*-induced expression changes drove the expression of the pink module more than any other network (Fig. 2d). Furthermore, both variation in *Zfp189* expression and variation in pink module expression were significantly correlated with resilient behavior ($R^2=0.48$, $P=0.026$ and $R^2=0.50$, $P=0.021$, respectively; Fig. 2e,f). Together, these data validate our bioinformatic predictions and indicate that the pro-resilient effects of *Zfp189* are preferentially associated with pink module gene expression in the PFC.

CREB is an upstream regulator of the resilience module. We next investigated how the pink module is regulated. We first used HOMER[16] to evaluate pink module genes for overrepresentation of known binding motifs in silico. Both activating transcription factor 1 (ATF1) and CREB are predicted upstream regulators of pink module genes (FDR $q=0.027$ and FDR $q=0.035$, respectively; Fig. 3a and Supplementary Table 3). The closely related ATF1 and CREB predictions bound near-identical CRE-containing consensus sequences, thus indicating that it is the CRE site that is overrepresented in the pink module. CRE-containing consensus sequences were unique to the pink module, with statistical enrichment of any binding site apparent in only 4 of the 29 other networks (FDR

$q < 0.05$; Supplementary Table 3), none of which contained this motif. Both ATF1 and CREB play important roles in cell survival[17] and are ubiquitously activated by extracellular signals[18], yet CREB has also been extensively implicated in both human MDD[19,20] and animal models of depression[21–24], while only non-ATF1 members of the ATF family have been implicated in stress responsivity[25].

To complement this analysis, we performed an upstream regulator analysis using ingenuity pathways analysis (IPA), which utilizes known interactions for a set of genes to determine upstream regulators based on downstream changes in expression. Matching our results with HOMER, we identified CREB as a predicted upstream regulator of pink module transcription across brain regions (Fig. 3b–e; Supplementary Table 4). In contrast, our HOMER finding of ATF1 regulation was not reproduced by IPA. While CREB is predicted to be more upregulated in susceptibility than resilience in the NAc, the BLA and the vHIP in our dataset, the predicted regulation of CREB in the PFC (up in resilient, no change in susceptible) mimics that of both pink module DEG enrichment and *Zfp189* differential expression (Fig. 1d). Therefore, we hypothesized that CREB might regulate the pink module in the PFC, in part, through direct interactions with *Zfp189*.

To investigate the role of CREB–*Zfp189* interactions in the pro-resilient regulation of the pink module, we analyzed a published chromatin immunoprecipitation with DNA microarray dataset of active, Ser133-phosphorylated CREB (pCREB) binding in the NAc following CSDS, which revealed that pCREB binding to *Zfp189* is reduced following CSDS and reversed following antidepressant treatment[23]. To determine human relevance, we performed qPCR analysis on postmortem PFC tissue samples from patients with MDD. While there was no effect of MDD on *CREB1* expression (Fig. 3f), *CREB1* mRNA levels were significantly correlated with *ZNF189* mRNA levels across samples in both control and MDD brains ($R^2 = 0.53$, $P < 0.001$ and $R^2 = 0.25$, $P = 0.018$, respectively; Fig. 3g). Moreover, there was a stronger positive relationship in control than MDD samples. As such, CREB–*Zfp189* interactions may be reduced in both human MDD and mouse CSDS.

CREB–*Zfp189* interactions regulate resilience. To evaluate our prediction that CREB drives resilience in the PFC, we injected $Creb^{fl/fl}$ mice with adeno-associated virus (AAV) expressing Cre recombinase plus GFP or GFP alone and exposed mice to a subthreshold social defeat test (Fig. 4a). In accordance with our prediction, AAV-Cre mice (functionally with a selective CREB knockout (KO) in PFC neurons) developed behavioral abnormalities in response to this social stress, but AAV-GFP control mice were unaffected (Fig. 4b). We next microdissected virally infected PFC and performed qPCR. Both *Creb1* and *Zfp189* levels were reduced in CREB KO mice (Fig. 4c,d), thus providing causal in vivo evidence of the regulation of *Zfp189* by CREB in PFC neurons.

Since our data indicated that CREB is upstream of *Zfp189*, that *Zfp189* promotes resilience and that *Zfp189* acts through changes in pink module expression, we reasoned that CREB KO in PFC neurons is pro-susceptible, at least in part, through the consequent reduction in *Zfp189*. If this is the case, concurrent overexpression of *Zfp189* should rescue the pro-susceptible effects of CREB KO. To evaluate this, we injected AAV-Cre in the PFC of $Creb^{fl/fl}$ mice while overexpressing either HSV-*Zfp189* or HSV-GFP and exposed mice to a subthreshold defeat test (Fig. 4e). Importantly, all cells infected by HSVs were previously infected by AAVs, thus indicating that *Zfp189* is overexpressed in neurons that lack CREB (Supplementary Fig. 6). Consistent with our previous findings, CREB KO mice injected with HSV-GFP showed social avoidance, whereas CREB KO mice supplemented with HSV-*Zfp189* did not (Fig. 4f). *Zfp189*-overexpressing CREB KO mice also exhibited higher sucrose preference than GFP-overexpressing CREB KO mice (Fig. 4g), further supporting the capacity of *Zfp189* overexpression to mitigate the pro-susceptible effects of CREB KO in the PFC.

While the pink module was identified from a dataset of male mice[3] and transcriptional effects of stress exhibit sex differences[8,26–28], we recently found that gene manipulations can induce similar behavioral effects even in the context of sex-specific transcriptional changes[29]. Therefore, we manipulated the PFC of female $Creb^{fl/fl}$ mice with AAV-Cre or -GFP plus either HSV-*Zfp189* or HSV-GFP and exposed mice to 6 days of subchronic variable stress (SCVS), a protocol that reliably induces depression-like behavior in female mice[8,26,27] (Fig. 4h). In the novelty suppressed feeding (NSF) test, CREB KO mice showed the longest latency to feed in the novel arena (Fig. 4i). While there was no difference in grooming time in the splash test or latency to immobility in the FST (Supplementary Fig. 7), CREB KO mice displayed significantly diminished sucrose preference (Fig. 4j). *Zfp189* overexpression blocked these effects of CREB KO, thus demonstrating that CREB KO increases stress susceptibility in females that, similar to males, can be rescued by concurrent *Zfp189* overexpression.

CRISPR-mediated CREB–*Zfp189* interactions promote resilience. Although our data suggested a functional relationship between CREB and *Zfp189* expression (Fig. 4c,d), indirect interactions between the two factors could be responsible. To more definitively evaluate the role of CREB–*Zfp189* interactions in resilience, and to probe the causal consequence of direct CREB action at the *Zfp189* gene in the PFC, we used CRISPR technology as a tool for locus-specific

Fig. 5 | CRISPR-mediated, locus-specific modulation of *Zfp189* with CREB or G9a bidirectionally controls resilient behavior. a, Schematic of the CRISPR vectors. The variable dCas9 functional moiety is in orange. The variable gene-targeting sgRNA is in yellow. **b**, Location of the *Zfp189*-targeting sgRNA binding site relative to other features in the *Zfp189* promoter (red). CRISPR vectors were packaged in HSV and delivered as a viral cocktail bilaterally to PFC. The box with the broken outline in the brain schematic denotes the field of confocal imaging for the far-left image in **c**. TSS, transcription start site. **c**, Immunohistological staining shows a high degree of colocalization of HSV-sgRNA expression vector (GFP) and HSV-dCas9 fusion expression vector (mCherry) in PFC neurons. Scale bars, 10× objective, 100 µm (far left); 20× objective, 50 µm (right three panels). Repeated with similar results in three animals. **d**, Quantification of virus colocalization of 10× objective confocal image in **c**. **e**, CRISPR-mediated targeting of active, pseudo-phosphorylated $CREB^{S133D}$ to *Zfp189* is sufficient to increase mRNA expression in the PFC relative to HSV-GFP, untargeted dCas9-$CREB^{S133D}$ and dCas9 with no functional domain targeted to *Zfp189* (Kruskall–Wallis test, $\chi^2(5) = 10.27$, $P = 0.036$, from left to right in figure panel: $n = 9$, 12, 5, 5 and 19 mice, two-tailed Mann–Whitney post-test $P = 0.035$, $P = 0.004$ and $P = 0.040$, respectively). Targeting dominant-negative $CREB^{S133A}$ to *Zfp189* has no effect. **f**, Experimental timeline to determine the effect of CRISPR-mediated placement of CREB at the *Zfp189* promoter in PFC neurons. **g**, Pro-resilient effects of CRISPR-dependent CREB–*Zfp189* interactions. dCas9-$CREB^{S133D}$ delivered with *Zfp189*-targeting sgRNA increases the time in the interaction zone when a target mouse is present relative to dCas9-$CREB^{S133D}$ with NT-sgRNA (mixed model ANOVA, virus $F_{1,76} = 6.235$, $P = 0.015$, $n = 38$ (HSV-NT-sgRNA) and 40 (HSV-*Zfp189*-sgRNA) mice, Bonferroni post-test $P < 0.05$). **h**, Targeting dCas9 with G9a to the *Zfp189* promoter reduces *Zfp189* expression (two-tailed *t*-test, $t = 2.835$, $P = 0.037$, $n = 6$ mice). **i**, Experimental timeline to determine the effect of CRISPR-mediated localization of G9a to the *Zfp189* promoter in PFC neurons. **j**, Pro-susceptible effects *Zfp189*-targeted repression with G9a. dCas9-G9a delivered with *Zfp189*-targeting sgRNA decreases the time in the interaction zone when a target mouse is present relative to dCas9-G9a with NT-sgRNA (mixed model ANOVA, interaction $F_{1,26} = 9.844$, $P = 0.0042$, $n = 13$ (HSV-NT-sgRNA) and 15 (HSV-*Zfp189*-sgRNA) mice, Bonferroni post-test $P < 0.01$). $^*P < 0.05$, $^{**}P < 0.01$. Bar graphs show the mean ± s.e.m.

editing; that is, to target the recruitment of CREB selectively to the *Zfp189* gene promoter in PFC neurons. We fused the nuclease-dead, RNA-guided, DNA-binding protein Cas9 to a constitutively active, phosphomimetic mutant form of CREB^{S133D} (dCas9-CREB^{S133D}) and designed single guide RNAs (sgRNAs) to target near the consensus CRE motif in the *Zfp189* promoter. The construct design is shown

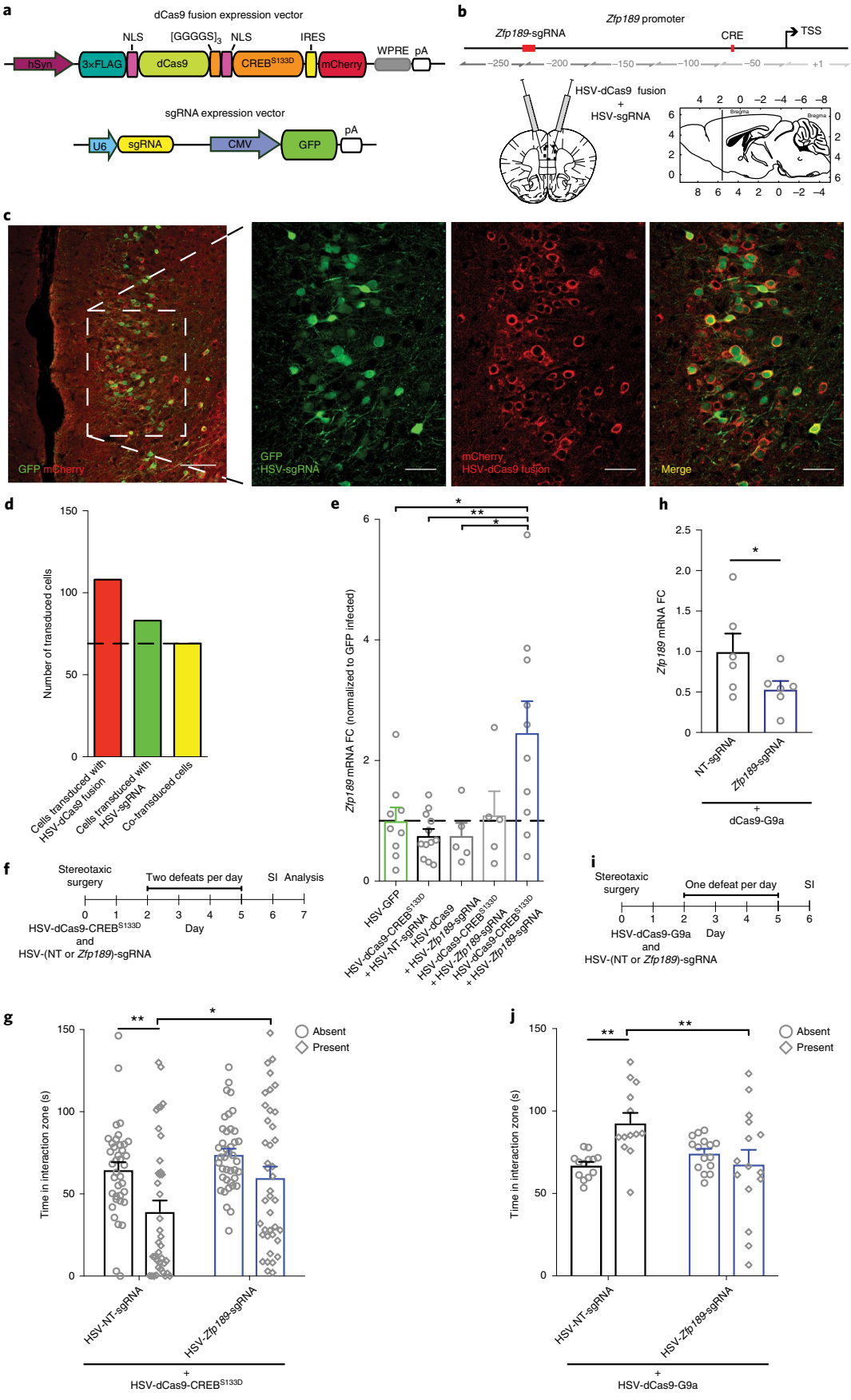

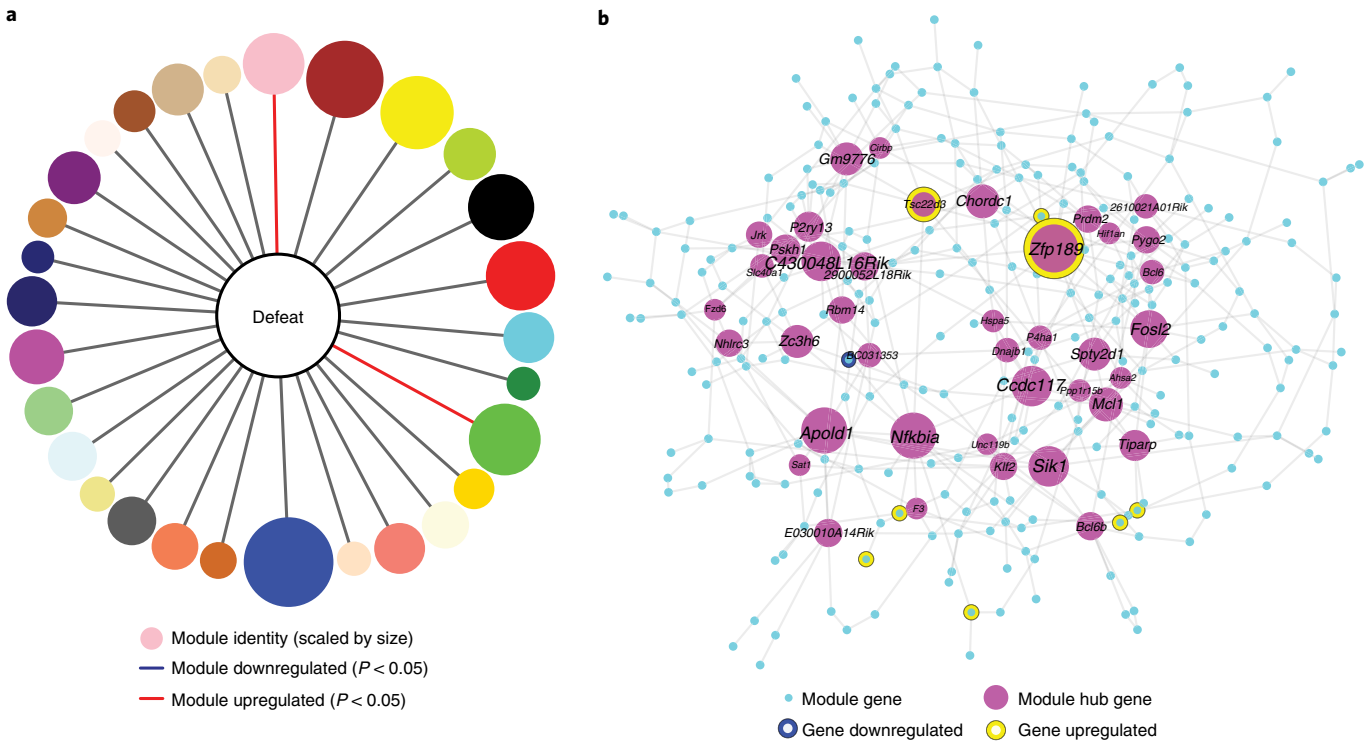

Fig. 6 | CRISPR-mediated induction of CREB–*Zfp189* interactions activates the pink module. a, Module overlap for PFC DEGs ($P < 0.05$, $\log_2(FC) > |0.2|$) resulting from *Zfp189*-targeted dCas9-CREB^{S133D} compared with NT-dCas9-CREB^{S133D} in mice exposed to social defeat. Enrichment was determined via multinomial logistic regression with Benjamini–Hochberg FDR correction for multiple comparisons as indicated. **b**, Pink module genes differentially expressed in defeated mice ($P < 0.05$, $\log_2(FC) > |0.2|$). $n = 20$ RNA-seq libraries consisting of unpooled samples from 8 *Zfp189*-targeted dCas9-CREB^{S133D} and 12 NT-dCas9-CREB^{S133D} mice.

in Fig. 5a. In vitro validation of sgRNAs showed that the top *Zfp189*-targeting sgRNA (*Zfp189*-sgRNA) induced *Zfp189* expression only when the active CREB^{S133D}, and not the phospho-null CREB^{S133A} or dCas9 with no functional moiety, is recruited to the *Zfp189* locus ($U = 1.0$, $P = 0.009$, $n = 5$–6; Supplementary Fig. 8). *Zfp189*-sgRNA targets dCas9-CREB^{S133D} ~150 base pairs upstream of the CRE motif in the *Zfp189* promoter (Fig. 5b). With the exception of the *Zfp189* locus, there is no complementary site in the mouse genome with fewer than three base mismatches, which suggests that there is a low in silico probability of off-target effects (Supplementary Table 5). Our control non-targeting (NT) sgRNA was also predicted not to target a specific sequence in the mouse genome (Supplementary Table 6).

We independently packaged our sgRNA expression vectors and our dCas9 fusion protein expression vectors in HSVs, and co-delivered these vectors to the mouse PFC. We observed that the two HSVs predominantly infected the same neurons (Fig. 5c,d), and targeting dCas9-CREB^{S133D} to the *Zfp189* promoter increased *Zfp189* expression in the mouse PFC (Fig. 5e). These data demonstrate the ability to harness the physiologically relevant mechanism of CREB-mediated induction of *Zfp189* expression with CRISPR-mediated transcriptional reprogramming in the mouse brain.

We next determined whether direct CREB-mediated activation of *Zfp189* is sufficient to promote resilience. We injected HSV-dCas9-CREB^{S133D} paired with either HSV-NT-sgRNA or HSV-*Zfp189*-sgRNA into the PFC and exposed mice to an accelerated social defeat stress procedure (Fig. 5f). In SI, mice with dCas9-CREB^{S133D} targeted to *Zfp189* showed significantly increased resistance to CSDS-induced social avoidance relative to mice with untargeted dCas9-CREB^{S133D} (Fig. 5g). Thus, inducing this single interaction between pCREB and *Zfp189* in PFC neurons is sufficient to increase resilience to social defeat.

We next determined whether an epigenetic modification that suppresses *Zfp189* expression prevents resilient-like behavior. To do this, we fused dCas9 to the repressive histone methyltransferase G9a (dCas9-G9a) and injected HSV-dCas9-G9a paired with either HSV-NT-sgRNA or HSV-*Zfp189*-sgRNA into the PFC. Directing G9a to the *Zfp189* promoter reduced *Zfp189* expression in the PFC (Fig. 5h). To determine the behavioral effects of this manipulation, we exposed mice to a subthreshold defeat condition of one 10-min defeat each day over 4 days and examined behavior in SI (Fig. 5i). As predicted, mice with dCas9-G9a targeted to *Zfp189* showed significantly decreased SI relative to mice with untargeted dCas9-G9a (Fig. 5j).

To test our hypothesis that these effects are associated with changes in pink module gene expression, we microdissected virally infected tissue from the dCas9-CREB^{S133D} experiment and performed RNA-seq (Supplementary Fig. 9a). Both the pink and green resilient modules were activated in response to CRISPR-mediated, CREB–*Zfp189* interactions in the context of social defeat ($P = 0.010$ and $P = 0.048$, respectively; Fig. 6a). Relative to traditional overexpression (Fig. 2a), we observed fewer regulated pink module genes overall (Fig. 6b), which is likely due to the more physiologically relevant levels of *Zfp189* induction (~2.5-fold *Zfp189* induction with CRISPR-mediated recruitment of CREB versus ~20-fold *Zfp189* induction with HSV overexpression).

To determine whether inducing CREB–*Zfp189* interactions in PFC neurons of unstressed controls is sufficient to produce similar changes in pink module genes, we repeated our dCas9-CREB^{S133D} injections in mice not exposed to CSDS (Supplementary Fig. 9). Again, the pink module was significantly affected when CREB is directed to the *Zfp189* promoter (FDR $q = 0.047$; Supplementary Fig. 9c), with a predominant upregulation of pink module genes (Supplementary Fig. 9d). Importantly, we did not observe regulation

of genes nearest to the 49 most homologous off-target sites of the *Zfp189*-sgRNA across the mouse genome in unstressed control animals, and regulation of only one off-target gene (*Tsc22d3*) in the defeat cohort, which is likely a result of the defeat experience itself (Supplementary Fig. 9e). These data substantiate the specificity of our CRISPR approach to direct CREB action at *Zfp189* alone.

Discussion

Here, we elucidated the higher-order organization of the transcriptional response to stress across limbic brain regions and demonstrated that a single, causal regulatory interaction can control activity of a phenotype-specific transcriptional network with definitive effects on complex behavior. Consequently, these data provide a mechanistic bridge between individual neuronal genes and the large-scale transcriptional response observed in resilience[2,3]. Taken together, our data show that the resilient-specific pink module is preferentially activated by *Zfp189*—the module's strongest driver gene—and that *Zfp189* (and thereby the pink module) is regulated by CREB in PFC neurons. As CREB–*Zfp189* interactions are impeded in both chronically stressed mice[23] and depressed humans (Fig. 3g), and promote resilience to CSDS (Fig. 5g,j), pharmacological manipulations of *Zfp189*, either directly or through CREB-dependent mechanisms, have the potential to regulate an entire network of pro-resilient genes and may be an attractive target for MDD therapeutics.

Because we showed that manipulations of either *Zfp189* (Fig. 2b) or CREB–*Zfp189* interactions (Fig. 6a) significantly affect the resilient-specific pink module, our findings are distinct from investigations of causal regulators of resilience to date that have focused on individual genes or molecular pathways[2,22,29–31]. Notably, our data support the existence of a transcriptional hierarchy, as we repeatedly showed that manipulation of one putative transcription factor (Zfp189), either directly or through epigenetic manipulations related to its upstream regulator CREB, is sufficient to increase resilience in multiple contexts (Figs. 2g–k, 4f,g,i,j and 5g) by activating a network of uniquely resilient genes. Even so, it is unlikely that the 281 genes in the pink module are the sole contributors to CSDS resilience, especially given the thousands of genes involved in the resilient response[2,3]. Consequently, there is likely some redundancy whereby multiple genes produce similar effects, and that the ability of the CREB–*Zfp189*–pink module axis to promote resilience occurs in the context of other molecular changes yet to be identified. Future studies are needed to address these possibilities.

Although our manipulations were initiated in neurons (Supplementary Fig. 3), some of the genes in the pink module are enriched in other cell types. For example, *Apold1*, which was the third-highest ranking key driver gene and was upregulated following HSV-*Zfp189* infection of PFC neurons selectively (Fig. 2a), is specific to endothelial cells[32]. These observations show that manipulations of *Zfp189* in neurons only cause downstream transcriptional effects in non-neuronal cell types through cell–cell signaling. While changes in the endothelium have been shown to play a role in CSDS susceptibility[33], the role of endothelial cells in resilience has not yet been defined. These findings illustrate the advantages of whole-tissue RNA-seq, as transcriptional relationships between cell types can be observed.

Our proposed mechanism for regulation of the pink module involves CREB activating *Zfp189* by binding to the *Zfp189* promoter. While we show that CREB KO in PFC neurons increases susceptibility, and that this can be mitigated with concurrent overexpression of *Zfp189* in the same cells (Fig. 4), this approach affects hundreds or thousands of genes, and it is impossible to discern whether our observed effects are due to altered CREB–*Zfp189* interactions or simply the pro-resilient effects of *Zfp189* obscuring the pro-susceptible effects of CREB KO. Most studies to date have relied on overexpression or knockdown strategies, which are limited in defining the exact causal mechanisms driving the progression of neuropsychiatric disease. To circumvent this problem and to more definitively characterize the role of regulatory interactions in controlling transcriptional networks, we employed CRISPR. While neuroepigenetic editing has been employed to answer questions related to neuropsychiatric disease[34–36], CRISPR technology provides a cheaper, more modular and more easily employable approach that can answer a wider array of relevant research questions and has been previously used to induce locus-specific epigenetic modifications in mammalian brain[37,38]. Our data demonstrate that CRISPR-dependent locus-specific epigenetic modifications can be used to mimic and block endogenously identified interactions and affect both downstream gene expression (Fig. 6; Supplementary Fig. 9c) and behavior (Fig. 5g,j).

Together, we have described a vital single molecular interaction of the known transcriptional regulator CREB and the novel downstream transcription factor Zfp189 that is capable of activating a network of genes in PFC neurons to mediate stress resilience. These findings elucidate the molecular mechanisms involved in stress resilience, as well as provide a broad molecular framework for the hierarchical organization and regulation of gene co-expression networks and their relationship to complex behavior.

Online content

Any methods, additional references, Nature Research reporting summaries, source data, statements of code and data availability and associated accession codes are available at https://doi.org/10.1038/s41593-019-0462-8.

Received: 8 November 2018; Accepted: 9 July 2019;
Published online: 19 August 2019

References

1. Berton, O. et al. Essential role of BDNF in the mesolimbic dopamine pathway in social defeat stress. *Science* **311**, 864–868 (2006).
2. Krishnan, V. et al. Molecular adaptations underlying susceptibility and resistance to social defeat in brain reward regions. *Cell* **131**, 391–404 (2007).
3. Bagot, R. C. et al. Circuit-wide transcriptional profiling reveals brain region-specific gene networks regulating depression susceptibility. *Neuron* **90**, 969–983 (2016).
4. Maschietto, M. et al. Co-expression network of neural-differentiation genes shows specific pattern in schizophrenia. *BMC Med. Genom.* **8**, 23 (2015).
5. Yue, Z. et al. Repositioning drugs by targeting network modules: a Parkinson's disease case study. *BMC Bioinformatics* **18**, 532 (2017).
6. Zhang, B. et al. Integrated systems approach identifies genetic nodes and networks in late-onset Alzheimer's disease. *Cell* **153**, 707–720 (2013).
7. Parikshak, N. N. et al. Integrative functional genomic analyses implicate specific molecular pathways and circuits in autism. *Cell* **155**, 1008–1021 (2013).
8. Labonte, B. et al. Sex-specific transcriptional signatures in human depression. *Nat. Med.* **23**, 1102–1111 (2017).
9. Malki, K. et al. Identification of genes and gene pathways associated with major depressive disorder by integrative brain analysis of rat and human prefrontal cortex transcriptomes. *Transl. Psychiatry* **5**, e519 (2015).
10. Margolin, A. A. et al. ARACNE: an algorithm for the reconstruction of gene regulatory networks in a mammalian cellular context. *BMC Bioinformatics* **7**, S7 (2006).
11. Zhang, B. & Zhu, J. Identification of key causal regulators in gene networks. *Proc. World Congr. Eng.* **II**, 5–8 (2013).
12. Covington, H. E. 3rd et al. Antidepressant effect of optogenetic stimulation of the medial prefrontal cortex. *J. Neurosci.* **30**, 16082–16090 (2010).
13. Odeberg, J. et al. Cloning and characterization of *ZNF189*, a novel human Kruppel-like zinc finger gene localized to chromosome 9q22-q31. *Genomics* **50**, 213–221 (1998).
14. Najafabadi, H. S. et al. C2H2 zinc finger proteins greatly expand the human regulatory lexicon. *Nat. Biotechnol.* **33**, 555–562 (2015).
15. Zeisel, A. et al. Brain structure. Cell types in the mouse cortex and hippocampus revealed by single-cell RNA-seq. *Science* **347**, 1138–1142 (2015).
16. Heinz, S. et al. Simple combinations of lineage-determining transcription factors prime cis-regulatory elements required for macrophage and B cell identities. *Mol. Cell* **38**, 576–589 (2010).
17. Bleckmann, S. C. et al. Activating transcription factor 1 and CREB are important for cell survival during early mouse development. *Mol. Cell. Biol.* **22**, 1919–1925 (2002).

18. Shaywitz, A. J. & Greenberg, M. E. CREB: a stimulus-induced transcription factor activated by a diverse array of extracellular signals. *Annu. Rev. Biochem.* **68**, 821–861 (1999).
19. Xiao, X. et al. The cAMP responsive element-binding (CREB)-1 gene increases risk of major psychiatric disorders. *Mol. Psychiatry* **23**, 1957–1967 (2018).
20. Juhasz, G. et al. The CREB1–BDNF–NTRK2 pathway in depression: multiple gene–cognition–environment interactions. *Biol. Psychiatry* **69**, 762–771 (2011).
21. Carlezon, W. A. J., Duman, R. S. & Nestler, E. J. The many faces of CREB. *Trends Neurosci.* **28**, 436–445 (2005).
22. Covington, H. E. et al. A role for repressive histone methylation in cocaine-induced vulnerability to stress. *Neuron* **71**, 656–670 (2011).
23. Wilkinson, M. B. et al. Imipramine treatment and resiliency exhibit similar chromatin regulation in the mouse nucleus accumbens in depression models. *J. Neurosci.* **29**, 7820–7832 (2009).
24. Chen, A. C., Shirayama, Y., Shin, K. H., Neve, R. L. & Duman, R. S. Expression of the cAMP response element binding protein (CREB) in hippocampus produces an antidepressant effect. *Biol. Psychiatry* **49**, 753–762 (2001).
25. Green, T. A. et al. Induction of activating transcription factors (ATFs) ATF2, ATF3, and ATF4 in the nucleus accumbens and their regulation of emotional behavior. *J. Neurosci.* **28**, 2025–2032 (2008).
26. Hodes, G. E. et al. Sex differences in nucleus accumbens transcriptome profiles associated with susceptibility versus resilience to subchronic variable stress. *J. Neurosci.* **35**, 16362–16376 (2015).
27. LaPlant, Q. et al. Role of nuclear factor kappaB in ovarian hormone-mediated stress hypersensitivity in female mice. *Biol. Psychiatry* **65**, 874–880 (2009).
28. Gray, A. L., Hyde, T. M., Deep-Soboslay, A., Kleinman, J. E. & Sodhi, M. S. Sex differences in glutamate receptor gene expression in major depression and suicide. *Mol. Psychiatry* **20**, 1139 (2015).
29. Lorsch, Z. S. et al. Estrogen receptor α drives pro-resilient transcription in mouse models of depression. *Nat. Commun.* **9**, 1116 (2018).
30. Vialou, V. et al. DeltaFosB in brain reward circuits mediates resilience to stress and antidepressant responses. *Nat. Neurosci.* **13**, 745–752 (2010).
31. Dias, C. et al. β-catenin mediates stress resilience through Dicer1/microRNA regulation. *Nature* **516**, 51–55 (2014).
32. Zhang, Y. et al. Purification and characterization of progenitor and mature human astrocytes reveals transcriptional and functional differences with mouse. *Neuron* **89**, 37–53 (2016).
33. Menard, C. et al. Social stress induces neurovascular pathology promoting depression. *Nat. Neurosci.* **20**, 1752–1760 (2017).
34. Heller, E. A. et al. Locus-specific epigenetic remodeling controls addiction- and depression-related behaviors. *Nat. Neurosci.* **17**, 1720–1727 (2014).
35. Hamilton, P. J. et al. Cell-type-specific epigenetic editing at the *fosb* gene controls susceptibility to social defeat stress. *Neuropsychopharmacology* **43**, 272–284 (2018).
36. Heller, E. A. et al. Targeted epigenetic remodeling of the *Cdk5* gene in nucleus accumbens regulates cocaine- and stress-evoked behavior. *J. Neurosci.* **36**, 4690–4697 (2016).
37. Liu, X. S. et al. Rescue of fragile X syndrome neurons by DNA methylation editing of the *FMR1* gene. *Cell* **172**, 979–992.e6 (2018).
38. Liu, X. S. et al. Editing DNA methylation in the mammalian genome. *Cell* **167**, 233–247.e17 (2016).

Acknowledgements

This work was supported by National Institutes of Health grants F30MH110073 (Z.S.L.), T32GM007280 (Z.S.L.), T32MH096678 (Z.S.L.), K99DA045795 (P.J.H), U01AG046170 (B.Z.), R01AG057907 (B.Z.), RF1AG057440 (B.Z.), P50MH096890 and R01MH051399 (E.J.N.), and by the Hope for Depression Research Foundation.

Author contributions

Conceptualization: Z.S.L., P.J.H., R.C.B. and E.J.N. Methodology: Z.S.L., P.J.H., I.O.T., H.G.K., S.E.M., I.M. and E.J.N. Software: Z.S.L., A.R., A.M., X.Z., Y.-H.E.L., B.Z. and L.S. Formal analysis: Z.S.L., P.J.H., A.R., X.Z., Y.-H.E.L., B.Z. and L.S. Investigation: Z.S.L., P.J.H., E.M.P., M.S., W.J.W., A.E.L., P.M., O.I., L.F.P., S.T.P., B.L., A.C. and A.E.S. Resources: A.M., R.L.N. and G.T. Writing (original draft): Z.S.L. and P.J.H. Writing (reviewing and editing): Z.S.L., P.J.H., R.C.B. and E.J.N. Visualization: Z.S.L., P.J.H., M.S. and X.Z. Supervision: I.M., Y.D., B.Z., L.S., R.C.B. and E.J.N. Project administration and research funding: E.J.N.

Competing interests

The authors declare no competing interests.

Additional information

Supplementary information is available for this paper at https://doi.org/10.1038/s41593-019-0462-8.

Reprints and permissions information is available at www.nature.com/reprints.

Correspondence and requests for materials should be addressed to E.J.N.

Peer review information: *Nature Neuroscience* thanks Cornelius Gross and the other, anonymous, reviewers for their contribution to the peer review of this work.

Publisher's note: Springer Nature remains neutral with regard to jurisdictional claims in published maps and institutional affiliations.

Methods

Animals. Experimental mice were either C57BL/6J mice or C57BL/6J mice that were genetically modified for a conditional brain region-specific Cre-dependent CREB KO by insertion of *loxP* sites flanking *Creb1* exon 2 (ref. [22]). In addition, 6-month-old CD1 aggressor mice were used as aggressors to induce social stress in the CSDS procedure, but were not included in any analysis. Wild-type C57BL/6J mice were 8 weeks old at the time of experimentation. $Creb^{fl/fl}$ mice were used between 8 weeks and 4 months of age due to breeding considerations, and age was counterbalanced across experimental conditions. C57BL/6J mice were housed five per cage, whereas CD1 mice were single-housed. C57BL/6J mice undergoing CSDS were single-housed following the final defeat, and C57BL/6J mice undergoing SCVS were single-housed following the final stressor. To maintain consistent study design, unstressed controls were single-housed at the same time as stressed mice. Once mice were single-housed, they remained as such until the end of experimentation. For all experiments, mice were randomized to experimental groups and only healthy, well-appearing mice were selected for experimentation. All mice were maintained on a 12-h light–dark cycle with lights on at 07:00 and a controlled temperature range of 22–25 °C. Food and water were provided ad libitum except for the 24 h preceding NSF testing, when food was removed. All experiments conformed to the Institutional Animal Care and Use Committee guidelines at Mount Sinai, which approved the animal experiments in the study. Behavioral testing took place during the light cycle of the animals. In cases where non-automated analysis was used, the experimenter was blinded to the experimental group. The order of testing in behavioral experiments was counterbalanced, and assignment to experimental groups was random.

Stress protocols and behavioral testing. CSDS and SI tests were performed according to established protocols[1,2]. CD1 retired breeder mice were screened for aggression in 3-min intervals over the course of 3 days. CD1 mice consistently attacking 8-week-old male C57BL/6J screener mice were included as aggressors for CSDS. On the first day of stress, a CD1 mouse were placed on one side of a large hamster cage separated by a perforated Plexiglas divider, and an 8-week-old male C57BL/6J mouse was placed on the other side. Importantly, this Plexiglas divider allows for sensory, but not physical, contact between CD1 and C57BL/6J mice. During each defeat, the C57BL/6J mouse was placed in the same side of the cage as the CD1 aggressor for a period of 7.5–10 min. This duration was kept constant throughout each experiment and was predetermined to titrate the defeat based on the overall aggression in the CD1 cohort during screening. During this time, the CD1 aggressor physically attacked the C57BL/6J mouse. Following the physical bout, the C57BL/6J mouse was returned to the other (empty) side of the divider where it remained in sensory contact with the CD1 aggressor that had just attacked it, but could not be further harmed physically. For each consecutive defeat session (24 h later for CSDS and subthreshold defeat and 12 h later for accelerated defeat), the C57BL/6J mouse was exposed to a new CD1 aggressor in a different hamster cage and the procedure was repeated. Control C57BL/6J mice were double-housed in a mouse cage separated by a perforated divider for the length of stress. To control for handling effects, control mice were moved to the adjacent half cage whenever a stress occurred for experimental mice. CSDS took place for a duration of 10 days, accelerated defeat took place over the course of 4 days with 2 defeats per day (to coincide with the time course of HSV-mediated transgene expression) and subthreshold defeat took place over the course of 5 days.

SCVS was performed as previously described[26] with three different hour-long stresses performed twice over a total of 6 days. Briefly, 8-week-old female C57BL/6J mice were exposed to foot shock (0.45 mA) on days 1 and 4, tail suspension on days 2 and 5, and restraint stress (in a 50-ml Falcon tube in the home cage) on days 3 and 6. Mice were group-housed (five mice per cage) when they were not being stressed, and control mice remained in their home cages throughout.

Behavioral tests occurred in a behavior suite different from where stress exposure was performed. In cases where a test was repeated following a manipulation, a different behavior room was used for the second test. Mice were given 1 h to habituate to the behavioral room before behavioral testing. Due to the timeline of HSV expression[39], multiple behaviors occurred on the same day when HSV vectors were used. To minimize spillover effects from one test to another, tests were separated by a minimum interval of 2 h. Behavioral analyses for SI, locomotion and OFT were performed automatically by video tracking software (Ethovision 10.0, Noldus). FST results were analyzed manually on pre-recorded video by investigators blinded to the study design, and sucrose preference test and NSF results were analyzed manually in real time. To ensure adequate power, sample sizes were chosen in accordance with the number of mice needed to show statistical significance in CSDS and SCVS conditions as defined by previous studies[3,26].

SI testing was performed under red light 24 h after the last social defeat stress. C57BL/6J mice were placed into an open arena with an empty wire cage at one side (interaction zone). Mice were given 2.5 min to explore the arena and then removed. A novel CD1 aggressor to which the C57BL/6J mouse had never been exposed to was placed in the cage (interaction zone) and the procedure was repeated. Time in the interaction zone was recorded automatically with video tracking software. Data were analyzed as time spent in the interaction zone when the aggressor was absent compared with time spent in the interaction zone when the aggressor was present. In cases where mice were subset into resilient and susceptible phenotypes, defeated mice with SI ratio scores >1.2 that spent >60 s in the interaction zone when the target was present were determined to be resilient. Defeated mice with SI ratio scores <0.8 that spent <40 s in the interaction zone when the target was present were determined to be susceptible.

OFT was performed by allowing mice 10 min to explore an open arena under red light. Although nothing was physically placed in the arena, the center and periphery were defined in video tracking software. The total time spent in the center was recorded and utilized for analysis. In addition, the total distance moved during this time was analyzed to determine locomotor effects.

The FST was always performed last in the sequence of behavior. FST was performed in 4 liter Pyrex beakers filled with 2 liters of 25 °C (±1°) water. Mice were placed in the water and recorded by a front-facing camera for a period of 6 min. Investigators blinded to the study design scored FST videos by recording the latency to the first immobility state.

NSF was performed following 24 h of food deprivation. Female mice were placed in a novel arena with corncob bedding and a single piece of food in the center of the arena. The time to feed was recorded manually under white light. Mice were given a maximum of 10 min to eat, after which the trial was ended and latency of 600 s was recorded. After the mouse ate in the novel arena, the mouse was returned to the home cage where a single piece of food was located in the center, and the time to eat in the home cage was recorded. Data were analyzed as the latency to eat in the novel arena and the latency to eat in the home cage.

The sucrose preference test was performed as a two-bottle choice test. One bottle was filled with water and the other bottle was filled with 2% sucrose. The initial weights of each bottle were recorded and bottle weights were recorded each morning and evening over the sucrose preference period. Sucrose preference was calculated as the change in weight of the sucrose bottle/the change in weight of both bottles × 100. Total sucrose preference was used for analysis.

To allow for peak viral expression at the time of behavior, AAV infusions and behavior were separated by 4 weeks, and HSV infusions and behavior were separated by 4–5 days, as described in the reported experimental timelines in the figure captions.

Tissue collection. Mice were killed 24 h after final behavior tests via cervical dislocation. To acquire only infected tissue within the PFC, microdissection was performed using a fluorescence microscope. Brain slices containing the PFC were either visualized on blade and directly punched or suspended in cold PBS before tissue dissection. PFC samples were collected as either a single midline 12-gauge punch or as bilateral 14-gauge punches, which varied according to virus spread. However, only the PFC was included in dissections. Mice were excluded from analysis when the PFC was not correctly targeted. Dissected tissue was immediately frozen on dry ice. Since our HSV and AAV vectors express GFP, there was no way to distinguish expression of the two viruses. As such, for experiments in which HSV and AAV vectors were both injected, the PFC was collected using a 12-gauge punch, and downstream qPCR with reverse-transcription was used to validate virus effects. In cases where dual 14-gauge punches were used, two punches (bilateral) from each mouse were combined, but samples were never pooled between mice.

Viral reagents. We overexpressed *Zfp189* using bicistronic p1005 HSV expressing GFP alone or GFP plus *Zfp189*. This involves a dual promoter approach whereby GFP expression is driven by a cytomegalovirus (CMV) promoter but *Zfp189* expression is driven by IE4/5. *Zfp189* was inserted into the p1005 plasmid from a plasmid containing the mouse *Zfp189* gene (Origene MR209370), which was packaged into HSV.

We overexpressed Cre recombinase in $Creb^{fl/fl}$ mice using AAV serotype 2 AAV-CMV-Cre-GFP virus from the University of North Carolina Vector core. Similar to expression of *Zfp189*, this virus induces Cre expression via the CMV promoter. In $Creb^{fl/fl}$ mice for which we intended to preserve CREB expression, we injected AAV-CMV-GFP (serotype 2).

We repurposed the CRISPR system to target CREB binding to the *Zfp189* promoter. We cloned and synthesized fusion constructs of a phosphomimetic mutant form of CREB or G9a fused to nuclease-dead *Staphylococcus pyogenes* Cas9 protein (dCas9-$CREB^{S133D}$ and dCas9-G9a, respectively), which can localize to specific sites along the genome based on the complementarity of a specific sgRNA sequence. sgRNA sequences for *Zfp189* were determined first in silica based on the sequence of the *Zfp189* promoter, and a suite of ten sgRNAs were designed to bind to distinct DNA sequences proximal to the CRE motif within the promoter. To promote specificity, sgRNA off-target effects were predicted using https://zlab.bio/guide-design-resources according to their published algorithm[40], and candidate sgRNAs with complementary sequences in the mouse genome with fewer than three base mismatches were excluded. The sequence of our NT-sgRNA (protospacer sequence: GCGAGGTATTCGGCTCCGCG) was identified from the GeCKO v.2 libraries and validated to ensure that no genomic site was targeted. All ten candidate sgRNAs were de novo synthesized as gBlocks from Integrated DNA Technologies containing a U6 promoter, a variable target sequence, a guide RNA scaffold and a termination signal. These were subcloned into a p1005 variant plasmid for HSV packaging. All *Zfp189*-sgRNAs were first validated in N2A cells to identify the most effective *Zfp189*-targeting sgRNA. Cells were transfected and

lysed after 48 h, and mRNA expression was analyzed by qPCR. The top sgRNA (protospacer sequence: GTGTCTCGGTTAGCAAGAAG) was packaged into HSV and tested in vivo.

In vivo confirmation of *Zfp189* induction was validated via qPCR on dissected PFC tissue. To minimize between-mouse variability, a hemispheric approach was utilized wherein the test constructs were injected into one hemisphere while control constructs were injected into the other hemisphere of the same mouse.

Viral-mediated gene transfer. Stereotaxic surgeries targeting the PFC were performed as previously described[3,41]. Mice were anesthetized with an intraperitoneal injection of ketamine (100 mg per kg) and xylazine (10 mg per kg) dissolved in sterile water. Subsequently, mice were placed in a small-animal stereotaxic device (Kopf Instruments) and the skull surface was exposed. Needles (33-gauge; Hamilton) were utilized to infuse 0.5 µl of virus at a rate of 0.1 µl min^{-1} followed by a 5-min rest period to prevent backflow. For $Creb^{fl/fl}$ and CRISPR experiments, 1 µl of virus at a rate of 0.2 µl min^{-1} was utilized to maximize viral spread within the PFC. The following coordinates were utilized for the PFC: from Bregma: anterior–posterior: +1.8 mm; medial–lateral: +0.75 mm; dorsal–ventral: −2.7 mm; 15° angle. While PFC injections targeted the infralimbic cortex, virus spread sometimes extended beyond these anatomical boundaries to other PFC regions.

Immunohistochemistry. Mice were anesthetized with an intraperitoneal injection of ketamine (100 mg per kg) and xylazine (10 mg per kg) and transcardially perfused with a fixative solution containing 4% paraformaldehyde (PFA) (w/v) in 0.1 M Na_2HPO_4/Na_2HPO_4, pH 7.5 at 4 °C delivered at 20 ml min^{-1} for 5 min with a peristaltic pump. Brains were post-fixed for 24 h in 4% PFA at 4 °C. Sections of 30-µm thickness were cut in the coronal plane with a vibratome (Leica) and stored at −20 °C in a solution containing 30% ethylene glycol (v/v), 30% glycerol (v/v) and 0.1 M phosphate buffer. Free-floating sections were processed for immunohistochemistry as follows. On day 1, sections were rinsed three times for 10 min in PBS before permeabilization for 15 min in PBS containing 0.2% Triton X-100 (Fisher). Sections were then rinsed three times in PBS followed by a blocking step of 1 h incubation in PBS containing 3% BSA. Primary antibodies against GFP (Aves Lab, GFP-1020, polyclonal: IgY lot: GFP879484, 1:500 dilution), mCherry (Abcam, ab125096, clone: 1C51, lot: GR3201780-3, 1:500 dilution), CD34 (Abcam, ab81289, clone: EP373Y, lot: GR201207-37, dilution 1:250) and NeuN (Abcam, ab104224, clone: 1B7, lot: GR3215839-1, dilution 1:500) were diluted in blocking solution and sections incubated overnight at 4 °C with gentle shaking. Sections were then washed three times in PBS and incubated with secondary antibodies (donkey anti-chicken Alexa Fluor 488, donkey anti-rabbit Cy3 or donkey anti-mouse Alexa Fluor 594; Jackson ImmunoResearch, 1:500 dilution) for 2 h at room temperature. After three rinses in PBS, sections were incubated for 5 min with 4,6-diamidino-2-phenylindole (DAPI; Sigma, D9542), washed again three times in PBS and then mounted in Vectashield (Vector Labs).

GFP and NeuN expression was assessed in the PFC using a LSM 710 laser-scanning confocal microscope (Carl Zeiss) imaged using a 10×, 20× or 40× oil immersion objective with a 1.0 digital zoom.

RNAscope. Fluorescent in situ hybridization (FISH) for *Rbfox3* (*NeuN*) mRNA (no. 313311) and *Zfp189* mRNA (no. 569561) was performed using a RNAscope Fluorescent Multiplex 2.0 assay as per the manufacturer's instructions (Advanced Cell Diagnostics)[42]. Briefly, fresh whole mouse brains were embedded in OCT medium and quickly frozen in 2-methylbutane chilled to −80 °C. Cryosections (20 µm) of PFC were than prepared and mounted on SuperFrost Plus slides. Sections were fixed and pretreated according to the RNAscope guide for fresh frozen tissue. After pretreatment, sections were hybridized with FISH probes using a HybEZ Hybridization System. After several amplification sets, the sections were counterstained with DAPI and mounted using Prolong Gold. Reactive cells were analyzed bilaterally in the NAc. Confocal images were acquired on a LSM 710 confocal microscope (Carl Zeiss) using a 40× or 63× oil immersion objective.

RNA isolation, qPCR, library preparation and sequencing. Total RNA was isolated from frozen dissected PFC tissue using QIAzol lysis reagent and purified using a miRNAeasy mini kit (Qiagen). Following isolation, RNA to be utilized in qPCR was quantified by Nano Drop (Thermo Fisher) and converted to complementary DNA with iScript (Bio-Rad). qPCR samples were analyzed in triplicate using the standard ΔΔCT method. For non-CRISPR experiments, hypoxanthine phosphoribosyltransferase 1 (*Hprt1*) was utilized for normalization for both mice and humans, and for CRISPR experiments, gene expression was normalized to the geometric mean of *Hprt1*, dCas9 and GFP transcripts to account for both cell health and appropriate delivery of tool components. For RNA being utilized for RNA-seq, RNA integrity (RIN) was assayed using an Agilent 2100 Bioanalyzer (Agilent). Average RIN values were above nine, and samples with RIN values less than eight were excluded from analysis. Each sample consisted of PFC punches from the same animal with no pooling between animals. Not all mice within each experiment were processed for RNA-seq. Samples utilized for sequencing were determined in all cases by the quality of the viral targeting and the quality of the resulting RNA (as determined by the RIN value). Additionally, in cases where the transcriptional effects of a particular behavior were being analyzed, samples that represented the group phenotype (overall effect) were selected for sequencing. For CRISPR experiments, only samples in which the effect of the CRISPR manipulation could be demonstrated were included in the analysis. RNA-seq of the effects of *Zfp189* expression included five samples per group (five HSV-*Zfp189* and five HSV-GFP) for previously susceptible mice and four to five samples per group (five HSV-*Zfp189* and four HSV-GFP) for unstressed controls. RNA-seq of CRISPR-infected tissue included three samples per group (three dCas9-$CREB^{S133D}$ + NT-sgRNA and three dCas9-$CREB^{S133D}$ + *Zfp189*-sgRNA) for undefeated controls and 8–12 samples per group (12 dCas9-$CREB^{S133D}$ + NT-sgRNA and eight dCas9-$CREB^{S133D}$ + *Zfp189*-sgRNA) for defeated mice. Libraries were prepared using a TruSeq RNA Sample Prep kit v2 (Illumina). Briefly, mRNA was polyA selected from the total RNA pool. mRNA was then fragmented and converted to cDNA with reverse transcriptase followed by cDNA size selection and purification with AMPure XP beads (Beckman Coulter). To identify each sample, strand-specific adapters were ligated to adenylated 3′ ends and an additional size-selection step was performed. The cDNA library was then amplified using PCR. During this step, barcodes of six base pairs were added to the adaptors. Library quality and concentration were measured using the Bioanalyzer before sequencing. Libraries were sequenced by either the Genomics Core Facility of the Icahn School of Medicine at Mount Sinai (*Zfp189* overexpression) using an Illumina HiSeq 2500 System with v3 chemistry and 100 base pair single-end reads or GENEWIZ (CRISPR sequencing) using an Illumina HiSeq System with 150 base pair paired-end reads. Multiplexing was performed to ensure minimum reads of 20 million for each sample.

RNA-seq. Raw reads obtained from PFC samples were mapped to mm10 using HISAT2 (ref. [43]). SAM files were converted to BAM files and were sorted according to chromosome number using SAMTools[44]. Counts of reads mapped to genes were obtained using HTSeq-count[45] against Ensembl v90 annotation. Differential expression analysis was carried out using the R package DESeq2 (ref. [46]). For virally infected tissue, sequenced samples in which the overexpressed transgene could not be adequately detected (*Zfp189* for HSV-*Zfp189* or dCas9, sgRNA or *Zfp189* for CRISPR studies) were considered to be a result of experimenter error (viral targeting or tissue selection) and were removed from analysis.

Identification of resilient-specific co-expression networks. To identify gene networks implicated in resilience, we utilized a previously published dataset[3] from our group that reported WGCNA modules and DEGs following CSDS. Briefly, WGCNA modules and differential expression profiles were generated from RNA-seq data with tissue taken at three time-points after 10 days of CSDS. Mice were exposed to stress, phenotyped in the SI test, and the PFC, NAc, vHIP and BLA were dissected for RNA-seq. Differential expression comparisons were region-specific, but brain regions were pooled before WGCNA. As such, reported WGCNA networks represent relationships of genes across brain regions.

Resilient modules presented herein are identical to the resilient modules presented in the supplementary material of our previous study[3] (Supplemental Table 3). Also, DEGs from the Supplementary Information were utilized for enrichment analysis, and unprocessed data were utilized to generate module structures with additional analyses as necessary.

Our approach to identifying resilient-specific co-expression networks was predicated on our hypothesis that resilient-specific modules would be both unique to the resilient phenotype and transcriptionally active immediately following CSDS. As such, we first examined the 30 resilient modules for MDC[6]. MDC is a measure of how connectedness among a set of genes is altered in the same genes in a different condition. This was performed as previously described[3] and modules with FDR $q < 0.05$ are reported as significantly differentially connected. However, while previous studies from our group[3,8] have identified networks for functional validation based on MDC in a single condition, gene expression[3,23] and circuit[47] alterations in the resilient phenotype are distinct from that of susceptibility or control and, therefore, only networks that showed MDC when compared with both phenotypes were considered resilient-specific.

Module enrichment analysis. To identify statistical overlap between previously identified differentially expressed genes (Gene Expression Omnibus (GEO) database: GSE72343)[3] and modules, we utilized the R package Super Exact Test (SET)[48]. The SET evaluates multi-set interactions to determine the difference between observed and expected overlap, which is then quantified statistically as an enrichment *P* value and fold change. Expected overlap for two gene sets is dependent on the size of the gene sets and the number of total variables in the dataset (background number of genes). Higher than expected overlaps are indicated by larger fold change values, which represents the ratio of observed overlap to expected overlap. SET is advantageous in this setting, as enrichment for upregulated and downregulated genes can be determined separately. PPIs were determined using STRING (v.10.5)[49].

Human brain analysis. To identify whether our resilient mouse modules were preserved in human brain, we used the modulePreservation function of the R package WGCNA to compare module identity in mouse to RNA-seq data from human control and human MDD data (GEO dataset: GSE102556)[8]. All brain regions included in the human analysis were included, and male and female

subjects were combined. To evaluate the difference between preservation in human controls and human MDD, we compared module preservation *P* values in each condition. A tenfold change in *P* value was considered to be a detectable deviation.

To evaluate *CREB1* and *ZNF189* levels in human brain, we used qPCR on reverse-transcribed mRNA from BA25, the PFC region most homologous to the ventral medial PFC targeted in our mouse studies. Samples from individuals with alcohol in their blood at the time of death were excluded due to possible effects on the transcriptome in the PFC. Demographics of the final cohort are shown in Supplementary Table 2. There were no significant differences in any of the demographics between MDD and controls. Experiments were conducted in accordance with the guidelines of the Douglas Institute Research Ethics Board. However, no specific ethical approval or guidance was provided for analysis of existing postmortem tissue.

Identification of the pink module network structure. We generated a network structure for the pink module using the algorithm for the reconstruction of accurate cellular networks (ARACNE)[10]. Critically, however, ARACNE is not a directed analysis, so connections between genes are still based on correlations. To attempt to resolve regulatory genes within the pink module, we next performed key driver analysis[11] on the ARACNE reconstructed network. Key driver analysis is predicated on the understanding that more important regulatory genes will have a larger effect on other genes in the module. Therefore, more important genes should forge more direct connections in the final module structure than less important genes. We analyzed the pink module structure at a threshold of two layers to identify the most important regulatory genes. Key driver genes had a number of connections that were significantly above the average value for the network and were considered for further in vivo analysis.

Identification of the relationship between *Zfp189* and the pink module. To establish the relationship between *Zfp189* and the WGCNA modules, we first obtained gene expression levels from the regularized log-transformation of DESeq2. The expression of each gene was then standardized to have zero mean and unit standard deviation across all samples. Principal component analysis was performed on each module (excluding *Zfp189*) to obtain the PC1 after weighting as the 'eigen-gene' for each module. The Pearson's correlation analysis was then performed between *Zfp189* and each module's eigen-gene to obtain the R^2 score.

Determination of pink module upstream regulators. To probe the pink module for specific regulatory binding sites, we utilized HOMER motif analysis[16]. HOMER examines binding sites within a gene set to see whether a specific binding motif is significantly enriched compared with what would be expected in a background gene set (in our case, the entire mouse genome). HOMER motif analysis was performed on all resilient modules. As such, we utilized a FDR cut-off of $P < 0.05$ for significant upstream regulators. To reduce the detection of false positives, we limited our candidates to known binding motifs.

To complement motif analysis, we performed upstream regulator analysis using the upstream regulator tool in Qiagen's Ingenuity Pathway Analysis (IPA; www.qiagen.com/ingenuity). This function predicts the identity and direction of change of known upstream regulators for a given differential expression signature from the magnitude and scale of gene expression changes in a dataset. Predictions used in this study were based on experimentally observed interactions within all datasets in IPA with the stringent filter setting applied. Reported *P* value calculations were determined from the Ingenuity Knowledge Base reference set considering both direct and indirect relationships. Any regulator for which there was sufficient evidence to generate an activation/inhibition prediction is reported. Input to IPA was prepared from transcriptional changes determined by RNA-seq in 48 h after CSDS (GEO database: GSE72343)[3]. Data were filtered for protein-coding genes. Three separate comparisons (susceptible versus resilient, resilient versus control and susceptible versus control) were utilized, and fold change values for all pink module genes were included as input.

Evaluation of overlap between RNA-seq and resilient modules. To test the overlap between the RNA-seq differential list and the resilient modules, we used multinomial logistic regression to predict the module membership using gene expression changes as regressors. The gene expression changes are log fold changes (LFCs) from the differential analysis. To control for noise, we combined *P* values with LFCs by forcing them to zero when the *P* value is less than 0.05 to derive a so-called *P* value adjusted LFC (PLFC). To control for covariates, such as gene length and GC content, that may affect the differential analysis, we included the log-transformed basal gene expression (LBGE) as a covariate in the logistic regression. The LBGE is standardized to have a zero mean and the same standard deviation as the PLFC to facilitate optimization. In multinomial logistic regression, we used the turquoise module as the reference since it is the largest module and does not show overlap with the differential list. The coefficient of the PLFC from the regression analysis can be interpreted as the significance of the overlap, while the coefficient of the LBGE indicates the bias of the covariates.

Gene ontology. Gene ontology for biological pathways was determined in EnrichR with gene identities of DEGs[50].

Statistics. Statistics were performed in Prism v.5.0 and v.8.0 for Mac (GraphPad Software) and SPSS Statistics v.22 (IBM). No statistical methods were used to predetermine sample sizes, but our sample sizes were similar to those reported in previous publications[2,3]. Unless otherwise stated, measurements were taken from distinct samples. For all behavioral analyses, outlier detection was performed using a Grubbs test with an alpha value of 0.05, and statistical outliers were excluded from analysis. Because there is no non-parametric equivalent for repeated measures tests, in accordance with the literature, all SI and NSF data were analyzed using a mixed model analysis of variance (ANOVA) where one of the factors (that is, target present, target absent) was treated as a repeated measure. A three-factor analysis model was employed when there were either two behavioral conditions (control versus stress or pre-test versus post-test) or two viruses (HSV and AAV) in addition to the repeated measure. In other cases, a two-factor analysis model was employed. For all tests other than SI and NSF, Levene's test of variance was first utilized to ensure that the data met the assumptions necessary for parametric statistics. In cases where data met the assumptions necessary for parametric statistics, data from two groups were analyzed using a two-tailed students *t*-test, and data from three or more groups were analyzed with a one-way or two-way ANOVA. When data were from the same animal, paired or repeated measures were utilized. In cases where the data did not meet assumptions for parametric statistics, data from two groups were analyzed using an independent samples Mann–Whitney and data from three or more groups were analyzed with a Kruskal–Wallis test. In these cases, different groups were compared using independent samples Mann–Whitney tests as post-tests. For parametric statistics, Bonferroni tests were used as post-tests. For comparisons of two continuous variables, we used linear regression analysis, in which case the coefficient of determination (R^2) is reported. To compare linear regressions, we used analysis of covariance (ANCOVA). Data that survived multiple comparisons correction are indicated, and analyses presented with correction are specified in the text with the FDR values. Additional information can be found in the Nature Research Reporting Summary.

Reporting Summary. Further information on research design is available in the Nature Research Reporting Summary linked to this article.

Data availability

The RNA-seq data reported in the paper are deposited in GEO with the accession number GSE118317. Other data that support the findings of this study are available from the corresponding author upon request.

Code availability

Scripts and code utilized in the analysis of study data are available from the corresponding author upon request.

References

39. Neve, R. L., Neve, K. A., Nestler, E. J. & Carlezon, W. A. J. Use of herpes virus amplicon vectors to study brain disorders. *Biotechniques* **39**, 381–391 (2005).
40. Hsu, P. D. et al. DNA targeting specificity of RNA-guided Cas9 nucleases. *Nat. Biotechnol.* **31**, 827–832 (2013).
41. Hamilton, P. J., Lim, C. J., Nestler, E. J. & Heller, E. A. Viral expression of epigenome editing tools in rodent brain using stereotaxic surgery techniques. *Methods Mol. Biol.* **1767**, 205–214 (2018).
42. Wang, F. et al. RNAscope: a novel in situ RNA analysis platform for formalin-fixed, paraffin-embedded tissues. *J. Mol. Diagn.* **14**, 22–29 (2012).
43. Kim, D., Langmead, B. & Salzberg, S. L. HISAT: a fast spliced aligner with low memory requirements. *Nat. Methods* **12**, 357–360 (2015).
44. Li, H. et al. The sequence alignment/map format and SAMtools. *Bioinformatics* **25**, 2078–2079 (2009).
45. Anders, S., Pyl, P. T. & Huber, W. HTSeq—a Python framework to work with high-throughput sequencing data. *Bioinformatics* **31**, 166–169 (2015).
46. Love, M. I., Huber, W. & Anders, S. Moderated estimation of fold change and dispersion for RNA-seq data with DESeq2. *Genome Biol.* **15**, 550 (2014).
47. Friedman, A. K. et al. Enhancing depression mechanisms in midbrain dopamine neurons achieves homeostatic resilience. *Science* **344**, 313–319 (2014).
48. Wang, M., Zhao, Y. & Zhang, B. Efficient test and visualization of multi-set intersections. *Sci. Rep.* **5**, 16923 (2015).
49. Szklarczyk, D. et al. The STRING database in 2017: quality-controlled protein–protein association networks, made broadly accessible. *Nucleic Acids Res.* **45**, D362–D368 (2017).
50. Chen, E. Y. et al. Enrichr: interactive and collaborative HTML5 gene list enrichment analysis tool. *BMC Bioinformatics* **14**, 128 (2013).

nature research

Corresponding author(s): Eric J Nestler

Last updated by author(s): 06/28/2019

Reporting Summary

Nature Research wishes to improve the reproducibility of the work that we publish. This form provides structure for consistency and transparency in reporting. For further information on Nature Research policies, see Authors & Referees and the Editorial Policy Checklist.

Statistics

For all statistical analyses, confirm that the following items are present in the figure legend, table legend, main text, or Methods section.

n/a	Confirmed	
☐	☒	The exact sample size (*n*) for each experimental group/condition, given as a discrete number and unit of measurement
☐	☒	A statement on whether measurements were taken from distinct samples or whether the same sample was measured repeatedly
☐	☒	The statistical test(s) used AND whether they are one- or two-sided *Only common tests should be described solely by name; describe more complex techniques in the Methods section.*
☐	☒	A description of all covariates tested
☐	☒	A description of any assumptions or corrections, such as tests of normality and adjustment for multiple comparisons
☐	☒	A full description of the statistical parameters including central tendency (e.g. means) or other basic estimates (e.g. regression coefficient) AND variation (e.g. standard deviation) or associated estimates of uncertainty (e.g. confidence intervals)
☐	☒	For null hypothesis testing, the test statistic (e.g. *F*, *t*, *r*) with confidence intervals, effect sizes, degrees of freedom and *P* value noted *Give P values as exact values whenever suitable.*
☒	☐	For Bayesian analysis, information on the choice of priors and Markov chain Monte Carlo settings
☐	☒	For hierarchical and complex designs, identification of the appropriate level for tests and full reporting of outcomes
☐	☒	Estimates of effect sizes (e.g. Cohen's *d*, Pearson's *r*), indicating how they were calculated

Our web collection on statistics for biologists contains articles on many of the points above.

Software and code

Policy information about availability of computer code

Data collection	In addition to data directly collected by the experimenters for this study, data from two sequencing studies (Labonte et al. 2017 Nature Medicine; GEO GSE102556 and Bagot et al., 2006 Neuron; GEO GSE72343) were used and are specified in the text.
Data analysis	Freely available software: Raw reads obtained from PFC were mapped to mm10 using HISAT2. SAM files were converted to BAM files and were sorted according to chromosome number using SAMTools. Counts of reads mapped to genes were obtained using HTSeq-count against Ensembl v90 annotation. Differential expression analysis was carried out using the R package DESeq2. We generated a network structure for the pink module using the Algorithm for the Reconstruction of Accurate Cellular Networks (ARACNE). We performed Key Driver Analysis (KDA) on this network. In order to identify statistical overlap between previously identified differentially expressed genes, we utilized the Super Exact Test (SET) R package. Protein-protein interactions were determined using STRING version 10.5. To identify whether our resilient mouse modules were preserved in human brain, we used the modulePreservation function of R package WGCNA. To probe the pink module for specific regulatory binding sites, we utilized HOMER motif analysis. Gene Ontology for Biological Pathways was determined in EnrichR with gene identities of differentially expressed genes. Commercial software: We performed upstream regulator analysis using the upstream regulator tool in QIAGEN's Ingenuity® Pathway Analysis (QIAGEN Redwood City, www.qiagen.com/ingenuity). Prism 5 and Prism 8 (GraphPad) and SPSS version 22 for statistical analysis. Ethovision 10.0 (Noldus) was utilized for automated behavioral analysis. Custom R scripts: Used to test overlap between RNA-seq and established resilient modules (multinomial logistic regression) and to identify the relationship between Zfp189 expression and the pink module (principal component analysis followed by Pearson's correlation). Both analyses are described in depth in the methods section.

For manuscripts utilizing custom algorithms or software that are central to the research but not yet described in published literature, software must be made available to editors/reviewers. We strongly encourage code deposition in a community repository (e.g. GitHub). See the Nature Research guidelines for submitting code & software for further information.

Data

Policy information about availability of data

All manuscripts must include a data availability statement. This statement should provide the following information, where applicable:

- Accession codes, unique identifiers, or web links for publicly available datasets
- A list of figures that have associated raw data
- A description of any restrictions on data availability

"RNA-seq data reported in the paper is deposited in GEO with the accession number: GSE118317". "Further information and requests for resources and reagents, including custom R scripts used in this study, should be directed to and will be fulfilled by Eric Nestler (eric.nestler@mssm.edu)".

Field-specific reporting

Please select the one below that is the best fit for your research. If you are not sure, read the appropriate sections before making your selection.

☒ Life sciences ☐ Behavioural & social sciences ☐ Ecological, evolutionary & environmental sciences

For a reference copy of the document with all sections, see nature.com/documents/nr-reporting-summary-flat.pdf

Life sciences study design

All studies must disclose on these points even when the disclosure is negative.

Sample size	To ensure adequate power, sample sizes were chosen in accordance with number of mice needed to show statistical significance in behavioral paradigms as defined by previous studies. No statistical method was used to determine sample size.
Data exclusions	Outlier detection was performed for all behavioral analyses using a Grubbs test with an α-value of 0.05. Statistical outliers were excluded from analysis. Behavioral data were also excluded when virus' were targeted incorrectly. For human PCR data, samples for which there was alcohol in the body at the time of death were excluded from analysis.
Replication	Bioinformatic findings central to the study were replicated with transcriptional analysis from independent tissue as is explained in-depth in the manuscript text. Additionally, when possible findings from mouse were replicated in human brain tissue. Finally, key behavioral findings were replicated in subsequent experiments that repeated the same manipulation with increasing levels of mechanistic specificity. All attempts at replication were successful.
Randomization	All behavioral testing was counterbalanced across experimental groups, and assignment to experimental groups was random.
Blinding	Behavioral analysis was performed either automatically by video tracking software (Ethovision 10.0, Noldus) on pre-recorded video manually by investigators blind to study design, or manually in real time.

Reporting for specific materials, systems and methods

We require information from authors about some types of materials, experimental systems and methods used in many studies. Here, indicate whether each material, system or method listed is relevant to your study. If you are not sure if a list item applies to your research, read the appropriate section before selecting a response.

Materials & experimental systems

n/a	Involved in the study
☐	☒ Antibodies
☐	☒ Eukaryotic cell lines
☒	☐ Palaeontology
☐	☒ Animals and other organisms
☐	☒ Human research participants
☒	☐ Clinical data

Methods

n/a	Involved in the study
☒	☐ ChIP-seq
☒	☐ Flow cytometry
☒	☐ MRI-based neuroimaging

Antibodies

Antibodies used	Primary: GFP (Aves Lab, GFP-1020, Polyclonal: IgY, Lot: GFP879484, 1:500 dilution), mCherry (Abcam, ab125096, Clone: 1C51, Lot: GR3201780-3, 1:500 dilution),CD34 (Abcam, ab81289, Clone: EP373Y, Lot: GR201207-37, dilution 1:250) and NeuN (Abcam, ab104224, Clone: 1B7, Lot: GR3215839-1, dilution 1:500) Secondary: (donkey anti-chicken Alexa Fluor 488, donkey anti-rabbit Cy3, donkey anti-mouse Alexa Fluor 594; Jackson ImmunoResearch, 1:500 dilution)
Validation	All antibodies were validated by the manufacturer and were chosen based on their extensive use in the literature. Antibodies

were further validated for use in IHC by comparing fluorescence in regions of the brain overexpressing the antibody target (GFP or mCherry) and comparing the signal to uninjected regions of the brain where no GFP or mCherry would be expected to be present.

Eukaryotic cell lines

Policy information about cell lines

Cell line source(s)	Neuro-2a (ATCC CCL-131)
Authentication	We obtained low-passage cell lines from ATCC and froze aliquots in liquid nitrogen. To perform our CRISPR construct validations, we thawed a single aliquot and maintained the cell line for a maximum of ten passages. During this time, we completed our experimentation, routinely checked morphology by microscope to assess cell health and identify the state of the cells, and ran mycoplasma detection.
Mycoplasma contamination	Cell lines were repeatedly tested for mycoplasma contamination over the course of experimentation. No mycoplasma was detected.
Commonly misidentified lines (See ICLAC register)	No commonly misidentified cell lines were used.

Animals and other organisms

Policy information about studies involving animals; ARRIVE guidelines recommended for reporting animal research

Laboratory animals	Male and female 8 week old C57BL/6J mice, Floxed CREB mice (http://www.informatics.jax.org/allele/MGI:4460924) and 6-month old CD1 retired male breeders (CD1 aggressors) were housed at 22-25°C in a 12-hr light/dark cycle and provided food and water ad libitum. All tests were conducted during the light cycle. Experiments were conducted in accordance with the guidelines of the Institutional Animal Care and Use Committee at Mount Sinai.
Wild animals	No wild animals were used.
Field-collected samples	No field-collected samples were used.
Ethics oversight	All experiments conformed to the Institutional Animal Care and Use Committee (IACUC) guidelines at Mount Sinai, which approved the animal experiments in the study.

Note that full information on the approval of the study protocol must also be provided in the manuscript.

Human research participants

Policy information about studies involving human research participants

Population characteristics	Post-mortem BA25 from patients with major depressive disorder and matched controls were utilized for qPCR analysis. Both male and female brains were utilized and demographic and sample information is included in detail in the Supplement. Age of the samples ranged from 19 to 82 and antidepressants, alcohol, and drugs of abuse in the system at the time of death was noted.
Recruitment	Post-mortem tissue was obtained from the Douglas-Bell Canada Brain Bank through the McGill Group for Suicide Studies. Recruitment information can be found at http://douglasbrainbank.ca/
Ethics oversight	Experiments were conducted in accordance with the guidelines of the Douglas Institute Research Ethics Board. However, no specific ethical approval or guidance was provided for analysis of existing post-mortem tissue.

Note that full information on the approval of the study protocol must also be provided in the manuscript.